We would like to thank both reviewers for their comments. Our final response follows. It contains our reply to reviewer 1, our reply to reviewer 2, and an updated manuscript with the changes highlighted.

Reply to Reviewer 1

We thank the reviewer for their thoughtful evaluation of our paper, and the comments offered to improve it. Our replies follow. We use bold face for comments, normal face for our reply, and put changes to the manuscript in quotation marks, with italics indicating new text. Strikethrough text denotes deletion.

This manuscript describes how to incorporate the effective pressure computed by a subglacial hydrology model into a basal drag inversion. Three different sliding laws are used: (1) a linear sliding law that does not depend on the effective pressure, (2) a "Budd"-type sliding law and a (3) a Schoof sliding law that both depend on the effective pressure. The authors propose here to do an inversion based on the first sliding law (1), to get a good initial guess of basal sliding, then run a subglacial hydrology model for the winter season, which computes the basal melt rate and basal water pressure that is then used to invert for the basal friction parameters used by the two other laws (2) and (3). They find that the basal drag and sliding ratio (ratio between the surface and basal velocities) of the linear and Budd sliding laws are in good agreement, but that their results using the Schoof sliding law show higher spatial variability.

Overall, this manuscript is easy to read and the methods are explained in detail, so that this manuscript is accessible to readers that are not necessarily familiar with model inversions. While I enjoyed reading it, I would have liked to see more discussion on their results instead of focusing mainly on the technical aspect. In its current state, the manuscript is limited to the introduction of a new model and a new approach, which would be more suitable to GMD for example. I do think that there is potential here for more scientific discussion. I am also a bit puzzled by their results with the third sliding law (see below), and why the slip ratios are so different. Since the same viscosity parameters are used for all three models, if the basal velocities are the same, the surface velocities should also be the same. Since we are trying here to reduce the misfit between InSAR velocities and modeled surface velocities, I would expect to see the same basal sliding velocities in all three cases, and this is not what is found here.

1 Major comments

I have one main concern, I don't understand the results of the Schoof sliding law. I read several times the explanations (page 22), but I still don't understand why the results are so different.

First, and maybe I am wrong, I don't think we need to do a second inversion once we have a good estimate of basal drag (τb) and basal velocities (ub) because there are always ways to change the friction parameters of different sliding laws to end up with the same basal velocities. If this is achieved, then the surface velocities are the same since the internal deformation is the same irrespective of the sliding law. In other words, one can invert for basal friction using a linear sliding law, and then use the results of a subglacial hydrology model to constrain the parameters of a different law using the results of the first inversion without performing another inversion.

For example, here, the three sliding laws are:

$$\boldsymbol{\tau_b} = \beta^2 \boldsymbol{u_b}$$
$$\boldsymbol{\tau_b} = \mu_a N_+^p {U_b}^q \frac{\boldsymbol{u_b}}{U_b}$$
$$\boldsymbol{\tau_b} = \mu_b N_+ \left(\frac{U_b}{U_b + \lambda_b A_b N_+^n} \right)^{\frac{1}{n}} \frac{\boldsymbol{u_b}}{U_b}$$

and the authors invert for β in (1), μa in (2) and μb in (3). If we invert for β and compute Ub and N+, one can determine μa and μb by simply doing:

$$\mu_a = \frac{\beta^2 U_b}{N_+^p U_b^q}$$

and

$$\mu_b = \frac{\beta^2 U_b}{N_+ \left(\frac{U_b}{U_b + \lambda_b A_b N_+^{\frac{1}{n}}} \right)^n}$$

Using these values for μa and μb, the forward model should produce the same surface velocities and therefore the same misfit to observations. The only problem might be the smoothness of these fields. So, I guess I have 2 questions:

Why do we need such a complicated procedure, when a simple single inversion would potentially enough?

This was our initial approach. However, the issue of smoothness led us to consider whether the values determined using the algebraic approach reflected conditions at the ice sheet bed.

The aim of an inversion is not to simply find a field of basal drag that can reproduce surface velocities. Inversions problems are underdetermined, and there are an infinite number of possible solutions. Rather, the aim is to set-up the inversion problem such that the values of μa/μb are representative of physical properties of the bed. The constraint we have to solve this aim is that those properties need to be able to reproduce surface velocities. This is important as we run the model into the future, and use the inverted values in our coupled model to predict surface velocities through a summer melt season.

The linear inversion problem (as we formulate it, although different regularization schemes are possible) is to find the field β^2 that reproduces surface velocities, yet is sufficiently smooth. If we simplify the Budd sliding law by assuming p, q= 1, and then match the results to the linear sliding law, we are solving:

$$\beta^2 = \mu_a N \qquad (1)$$

We don't think this is a physical relationship. It is illustrative to look at the limit of N→0 (e.g. a subglacial lake). In that case, this formula tells us that μa→Inf. We don't interpret this value of μa as reflecting physical properties of the bed. A nearby cell where N ~ 1MPa would have a much different value of μa. However, geologically, we would anticipate the properties of the bed beneath a lake and at a nearby location to be similar. Similarly the results of the inversion should be resilient to small changes. If we invert before a subglacial lake drains, and after a subglacial lake drains, we would want to recover similar values of μa/μb in that location. This is not possible with the algebraic approach. By using Equation 1, the results also take on the assumptions made by the regularization, that the product of effective pressure and bed properties should vary smoothly. We feel that this isn't the best assumption we can make.

The approach we propose states a different problem. We assume we know N. We invert for μa/μb. We still have to regularize the problem, but in this case, the regularization is stating that the bed properties vary smoothly. This is a more physical and justified assumption in our perspective. In areas where N→0, the regularization enforces that μa/μb vary smoothly. It also possible that we may at some point have a-priori information about μa/μb or N via measurements. This approach would allow us to incorporate this information via different/additional regularization. For instance, rather than assume μa/μb vary smoothly, we may want to minimize the difference from a background value.

Each of the inversions for the different sliding laws is a different problem. Here, we are using the linear inversion to be able to predict N. Then we incorporate this information into the problem relating to the values of μa/μb. The algebraic approach may be a practical alternative for predicting the values of μa/μb under conditions when the magnitude of N has limited variability and varies smoothly. Although the effective pressures shown in the manuscript have those properties, the output of the subglacial hydrology model is sensitive to the parameters used. With plausible parameters, we observed N→0 and vary by orders of magnitude. This required us to generate a general approach. A continuum model of subglacial hydrology also leads to a smooth solution. Different formulations of subglacial hydrology may result in higher and more rapid variations of N.

On a practical note using Equation 1, with N=0, leads to μa=NaN. You have a problem of infilling these locations. This does not happen in our procedure, as in this case, μa/μb have no impact on the first term of the cost function (least squares misfit), and are determined by the second term in the cost function (smoothness).

Why are the results of the Schoof sliding law so different? Is it because the inversion converged in a local minimum?

Comments from both reviews led us to scrutinize our explanation in greater detail. Previously we had done a simple calculation which showed that N was in the order of magnitude where the sliding law was in the Coulomb limit. However, when responding to the comments, we plotted the transition point for a range of N and U, and found that the Schoof sliding law was not in the Coulomb limit for the range of velocities and effective pressures in our domain.

Unfortunately, there was a discrepancy between the text and figure. While wrote in the text that the results were from \gamma_2=1e11, we had plotted the results of \gamma_2=1e09. The higher frequencies observed are not due to the sliding law, but because of a discrepancy in regularization. We have updated the figure with the results we intended to show, which are now similar to the other sliding laws.

Text has been updated as follows:

[Non-linear sliding laws subsection of Results] Page 18, 10-11 Lines + Page 21 Lines 1-3

~~"Figure (14 and 17) show the inversion results from the Weertman and Schoof sliding law respectively. Inverted basal drag using the Weertman sliding law is very similar to the results from the linear sliding law. In contrast, the inverted basal drag from the Schoof sliding law shows much higher frequency and magnitude spatial variations. This is reflected in the spatial distribution of the sliding ratio, with the Weertman sliding law resulting in a distribution similar to the linear sliding law, while the distribution from the Schoof sliding law shows much greater variation."~~

"Figure 5 shows the inversion results from the Budd and Schoof sliding laws. Inverted basal drag and the consequent sliding ratio using the two non-linear sliding laws are very similar to the results from the linear sliding law. Model mismatch is also similar for all three sliding laws (Figure 4)."

[Results Section] Page 22, Lines 7-19

~~"The pattern of basal drag inverted using the linear and Weertman sliding law show limited differences. This is due to the fact that basal shear traction must satisfy the global stress balance (Joughin et al., 2004; Minchew et al., 2016). Both the linear and Weertman sliding law have the form $\tau b = C \cdot u1/m$ in the inversion, since effective pressure can be incorporated into the constant C for the Weertman sliding law. Previous work shows that in this case $C \propto u-1/m$, and the recovered fields of basal drag are within a few percent of each other (Minchew et al., 2016). The basal drag and basal velocities from the the linear sliding law to initiate the subglacial hydrology model are therefore self consistent with the subsequent inversion results of the Weertman sliding law. The pattern of basal drag inverted using the Schoof sliding law however, shows both higher spatial variability and a higher magnitude of variability. This is a result of the Schoof sliding law shifting to Coulumb-like behaviour at low effective pressures."~~

"The pattern of basal drag inverted using the three different sliding laws show limited differences. This is due to the fact that basal shear traction must satisfy the global stress balance \citep{Joughin2004, Minchew2016}. The basal drag and basal velocities from the linear sliding law used to initiate the subglacial hydrology model are therefore self consistent with the subsequent inversion results of the two non-linear sliding laws. For the winter effective pressures predicted by the subglacial hydrology model, we find that the Schoof sliding law is in the viscous drag regime. For a representative basal velocity of 75 \unit{m yr^{-1}}, the transition to Coulomb friction occurs at effective pressures of approximately 0.7 MPa. This is below modelled effective pressures, which are above 1.3MPa for most of the study domain."

It would be nice to try and start with the μa and μb from equations 4 and 5 and see if you indeed get the same sliding ratio for all 3 sliding laws.

We hope that our discussion above illustrates that while this can be done on a technical level, the approach we propose is more general.

2 Specific comments

- **p3 equations 3, 4 and 5: I think you are missing a minus sign for all these equa- tions (basal drag opposes motion)**

  This form appears commonly in the literature [e.g Hewitt (2013)]. We subtract basal drag in the momentum equations.

- **p3 eq 5: use \left(\right) rather than simple parentheses.**

  Fixed

- **p3 l20: I would rather call this equation a Budd sliding law since he is the one**

  who introduced effective pressure in basal stress.

  Updated throughout.

- **p3 l24: you should take the norm of τb here (not the vector) since you are com- paring to a scalar**

  Fixed

- **p4 eq 6: minus sign missing here two?**

  See note above

- **p4 l8: maybe mention "outward pointing"**

  Included

- **p6 l27: "is the control parameter." (period missing)**

  Fixed

- **p7 l11: exp (ζ (x, y)). (parenthesis missing)**

  Fixed

- **p8 l4: with respect to the initial input**

  Updated

- **p8 eq 26 and 27: I think you should use capital Bi at the numerator since your are deriving the function, not its output. Equation 26 should therefore be**

  $$\delta J = \left(\prod_{i=N}^{1} \frac{\partial B_i}{\partial b_{i-1}} \right) \frac{\partial B_0}{\partial \phi_i} \delta \phi_i$$

  updated equations

- **p8 l27: to generate a *derivative*?**

  Fixed

- **p8 l29: derivative?**

  Fixed

- **p9 l2: gradient of *a* function**

  Fixed

- **p9 l6: forward accumulation AD tool: I think this method is generally referred to**

  as “Object Overloading”

  Forward accumulation refers to the general idea/concept, while “Object Overloading” refers to a specific method of implementing forward accumulation.

- **p12 l9: 500 m (space missing)**

  Fixed

- **p13 l2: An L-curve analysis**

  Fixed

- **p15 figure 14: I think what matters is not so much that the sliding laws 2 and 3 are non linear, what is important here is that they depend on the effective pressure, so I would replace the third box to “Inversion: effective pressure-dependent sliding Law”.**

This is a good point. We have removed the flow chart in response to comments from Reviewer 2, but have incorporated this comment in a manuscript in preparation.

- **p16 l2: 500 m (space missing)**

  Fixed

- **p17 l1: the the**

  Fixed

- **pp17 l15: maybe mention water sheet thickness?**

  Updated to “The maximum distributed system sheet thickness”

- **p17 l17: is it really mPa or MPa?**

  Mpa, fixed

- **p18 l10: Figure 14 and 17 (no parentheses needed)**

  Fixed

- **p22 l2: will account for some of the effects, which would (comma missing)**

  Fixed

- **p23 l1: hydrology runs are reflective**

  Fixed

- **p28 l6: we would like to thank M. ...**

  Fixed

Reply to Reviewer 2

We are pleased that reviewer thought this was a worthwhile study, and appreciate the constructive comments. Our replies follow. We use bold face for comments, normal face for our reply, and put changes to the manuscript in quotation marks, with italics indicating new text. Strikethrough text denotes deletion.

General comments:

This study is an investigation of hydrologically-forced ice-flow model initialization using multiple inversions for basal drag. It explores three commonly-used sliding-law formulations in attempting to initialize seasonal runs with an end-of-winter hydro-mechanical state. The general scientific question addressed is worthwhile for all the usual reasons of improving model fidelity to observations and the need for practical and sensible means of incorporating the effects of basal hydrology on ice-sheet dynamics. The paper is clearly written.

The paper appears to report on part of a PhD thesis that seems a fulsome combination of model development, numerical implementation and glaciological application. Presumably for this reason, the paper has excessive detail in some places (particularly where the model development appears to mimic previous work) and omission of detail elsewhere where it would be warranted. The paper could also make better use of space with many of the figures. A related consequence of the paper's origin is that it skates over the scientific justification for the development of a new ice-flow model that seems to implement what is already in the literature. One can imagine the reason for this: the author(s) coded this part of the model from scratch, but used existing code for the coupled hydrology. This is an excellent experience for a PhD student, but now the task of the authors is to justify to the scientific community why the world needs another ice-flow model, and this one in particular.

One of the main results of the paper is that using a Coulomb-friction-type sliding law, with a modelled distribution of effective pressure, yields a markedly different distribution of basal drag (and therefore sliding rate) than using a linear sliding law. This result is closely tied to the behavior of the hydrology model, and presumably to the parameters used in the sliding law. The differences are explained in terms of the non-linearity of the sliding law and its sensitivity to effective pressure, as well as the continuum nature of the hydrology model. The dependence of this result on model details warrants more emphasis on the parameters chosen for the hydrology model and Coulomb-friction sliding law, as well as the behavior of the latter.

This is a worthwhile study and I hope the comments below serve to improve the final paper.

Introduction of a new ice-flow model:

It appears that this depth-integrated model closely follows the work summarized in two sources (Goldberg, 2011; Arthern et al., 2013), with the novelty that the new model allows periodic boundary conditions (related to the ISMIP-HOM experiments). The authors even acknowledge that their model is more limited in some ways due to soft- ware (bottom of pg 6). Are there other departures from the two sources that could be highlighted as new innovations? How does this formulation differ or improve upon the coupled (also depth-integrated, if I recall) model of Hewitt (2013), whose hydrology model is employed in this study?

For the problem presented in this paper (a single season and a single catchment), one might legitimately ask why it wouldn't be better to simply use an existing code like Elmer/Ice, which includes a built-in inversion for basal friction and may well also include the hydrology model of Werder et al (2013):

http://elmerice.elmerfem.org/wiki/lib/exe/fetch.php?media=courses:elmerice_2015_friction.pdf

The numerics of the ice sheet model are not particularly novel. The model differs from that of Hewitt (2013) in that the momentum equations are written in terms of depth integrated velocities rather than basal velocities.

There are a variety of reasons to write a new ice sheet model. The reviewer has identified a primary motivation, which is to understand the numerics/equations. For this study, the ice sheet model/inversion code needed to include sliding laws not implemented in existing models and be coupled with the subglacial hydrology model of Hewitt (2013). At the beginning of the project, we were uncertain what this would entail in terms of links to any existing ice sheet model code, and pragmatically, writing the code from scratch ensured familiarity and flexibility of the code. Additionally, we have limited experience coding in low-level languages. Writing our own code allowed us to rapidly test model ideas/configurations, which could perhaps later be integrated in to more stable and full featured project such as ISSM / CISM / Elmer/ice. We haven't seen any publications from Elmer/Ice in regards to coupled modelling. Even so, subglacial hydrology model is in its early stage, and a diversity of models/approaches is beneficial to the community.

Imbalanced detail:

The basic governing equations, simplifications, boundary conditions and sliding-law formulations given on pp 3-5 are needed, but section 2.1.2 (Implementation) could be condensed, as it seems to closely follow Arthern et al (2015). Section 2.2 (Inversion) is long and detailed, particularly considering that it seems to closely follow Goldberg and Heimbach (2013). For example, the information in the text on pg 7, lines 1-18, is pretty standard fare for inversions, so could be shortened. Section 2.2.2 is detailed and didactic; is the discussion of the TLM necessary? It is nice to have a brief description of the adjoint model, but I expected most readers would be somewhat familiar with these methods already.

On the other hand, the hydrology model is fundamental to this study but is only briefly described (p 10, lines 2-10). The hydrology model seems as important as the numer- ical details of the ice-sheet model. Consider presenting the key governing equations here. Although the equations are currently absent, the hydrology model includes parameters whose values must play an important role in the results (p. 13, lines 7-9). It would be worthwhile reporting values for the cavity step height, the effective hydraulic conductivity/permeability and the incipient channel-width length scale, along with any other parameter settings that differ from Hewitt (2013) and Banwell et al (2016).

Further, the results and discussion would be more accessible if the reader knew a bit more about what went on with the hydrology model behind the scenes. For example, see p. 22, lines 4-6.

As the reviewer noted, there is a strong focus on the ice sheet model/inversion code details as this introduces a new code. However, the hydrology model is an 'off-the shelf' component.

We avoid detailed treatment of the hydrology model for a few reasons. The main innovation in this study from our perspective is the workflow, which is independent of the subglacial hydrology model. In this study, we use the model from Hewitt (2013) to generate the winter field of effective pressure. The parameters used are those we need to initiate summer runs based on calibration/validation of the integrated model using summer velocities. The winter results are an outcome of the summer calibration. Because the continuum model would not capture the fragmentation (as noted by the reviewer), the sheet thickness doesn't correspond to radar data, and due to a general lack of data on subglacial conditions, we don't scrutinize the winter hydrology output closely. Rather, the field of effective pressure is a-priori guess – plausible -- but not definitive for the above reasons.

This depends on your background, but our impression is that there is less familiarity with inversion procedures than subglacial hydrology in the community, as the latter lends itself to a conceptual understanding. From personal experience, understanding the methods behind inversions is involved. While the text was necessary for a thesis, our hope is that the in-depth writing could be useful for those without a background in adjoints. The crux in significantly cutting out sections would be that the paper remains verbose for experts, but not detailed enough for everyone else.

Overall, for reasons of length we think that only one of the models can be described in detail. There are good reasons for focusing on the ice sheet model/inversion code, although we acknowledge that some readers would benefit from the alternative choice suggested by this reviewer. Since reviewer one noted that our approach was accessible for readers without a background in inversions, we've decided to only make the minor changes suggested by reviewer one rather than rewrite the section.

Consider moving the two blocks of pseudocode into an Appendix. Likewise, the flow chart in Figure 4 could be omitted. There is a fair bit of blank space and redundancy in some of the figures. Here are some suggestions for a more efficient and impactful presentation:

Moved pseudocode to appendix, jettisoned flow chart.

- Combine Figs 2 and 3 (unlabeled E, N coordinate values can be removed from axis tick labels, as long as there is a scale bar) - Omit Figs 7a, 13a, 16a, or make them small insets in the corresponding b panels. - Omit or move to an appendix Fig 6. Nice to know how convergence occurs, but not necessary to show as a figure. - Combine Figs 8, 14, 17 into a single figure with 9 panels. This facilitates comparison. - Combine Figs 5, 12, 15. Could be done in a single panel figure. - Omit Fig 10. So much white space that could be replaced by a sentence. If it must be retained, consider a log plot.

We have:

A) Combined Figs 2 and 3.

B) Omitted figs 7a, 13a, 16a. Combined 7b, 13b, 16b into one figure with three panels.

Removed the text:

Page 17, Lines 1-6

"~~The histogram of the the difference between observed and modelled velocities (Figure 7) has a maximum in the lowest bin, with a rapid decrease into a long tail. The maximum difference is approximately 165 myr−1. The difference between modelled and observed velocities is less than 10 myr−1 for 88% of the cells in the study area, and less than 20 myr−1 for 96% of the cells in the study area.~~"

Page 18, Lines 6-9

"~~The histogram of the absolute difference between observed and modelled surface velocities for both non-linear sliding laws shows a similar distribution to the linear sliding law inversion (Figure 13 and 16). The Weertman sliding law results in a spatial distribution of misfit similar to the linear sliding law, while spatial distribution of error from the Schoof sliding law shows higher frequency variations. Model mismatch again is highest in the vicinity of the nunatak.~~ "

C) Omitted the plot of convergence.

Removed the text:

Page 17, Line 1

"~~The inversion converges in 46 iterations (Figure 6).~~"

D) Combined plots 8, 14, and 17

E) We have put figs 5,12, and 15 into a single plot with 3 panels. Overlaying them onto one panel obscured the scaling factors.

F) Omitted Figure 10

Removed the text:

Page 17, Line 13:

"~~Relative to discharge at the base, changes in effective pressures have a much lower magnitude.~~"

In addition, we have updated the colour palette in in some figures for consistency, removed the axis tick labels except in

Figure 1, and added a scale bar to figures which were lacking them.

Specific comments (page.line):

1.8: “a recent subglacial hydrology model” This sounds like it must be a different model than is used in the paper, but by the end it is clear that the model is that of Hewitt (2013). Please reword to clarify.

Apologies for the confusion, we hope this rewording of the last sentence eliminates the issue:

Additionally, we compare the modelled winter hydrological state to radar observations, and find that it is in line with summer rather than winter observations.

3.16 “Ab is the creep parameter set to an appropriate value for basal ice”. One should explain why the flow-law rate factor should be different by an order of magnitude (see Table 1) for basal ice, particularly in light of the differences in the results between the Coulomb-friction sliding law (which uses Ab) and the other two sliding laws.

Amended as:

“Ab is the ice creep parameter *used for basal ice. It set an order of magnitude lower than A to account for warmer ice at the base (following Hewitt (2013)). The value of Ab is used in both the Schoof sliding law, and in the subglacial hydrology model for determining creep closure of channels and cavities. The value of A is used in the momentum equations.*”

12.14: “the magnitude of the change is relatively limited” Pretty vague. Can this be quantified?

The scale in the figure of Colgan et al. (2012) is quite coarse, while the data in Van de Wal et al. (2015) are averaged over several seasons. However, from the latter paper we make a conservative estimate of <25%. The text is changed as follows:

*“*the magnitude of the change is *limited (<25%).”*

16.15: Why choose \gamma_2 = 10^{-12} rather than \gamma_2 = 10^{-11} in this type of trade-off curve?

The L-curve is a method for selecting the trade-off between model fit and regularization. Although a common selection is the point of maximum curvature, this choice is subjective, and often results in over smoothing: (*https://www.sintef.no/globalassets/project/evitameeting/2005/lcurve.pdf*)

Our selection of \gamma_2 = 10^{-12} is subjective, although Morlighem (2013) selected a similar point on the L-curve.

Morlighem, M., et al. "Inversion of basal friction in Antarctica using exact and incomplete adjoints of a higher‐order model." *Journal of Geophysical Research: Earth Surface* 118.3 (2013): 1746-1753.

17.15: “bed roughness scale of 0.5 m” refers to lambda_b?

We were not clear with our terminology here. The 0.5 m refers to the cavity height scale used in the subglacial hydrology model, which controls the maximum sheet thickness. We chose omit this detail and to simplify this sentence so it reads:

“The maximum distributed system sheet thickness is 0.36 \unit{m}.”

21.Fig 11b: Consider plotting pw/(rho_ice g h_ice) rather than (or in addition to) N, as N does not immediately reveal how close the bed is to flotation.

We think N is the appropriate field to plot as this is what we use in our sliding law. Since we don't discuss the hydrology model output in detail, plotting pw/(rho_ice g h_ice) isn't within the intended scope of the paper.

21.8-9: It seems intuitive that there would be a contribution from deformation, so what is going wrong in the simulations/inversions to produce a better match of observed and modelled surface velocities when the sliding ratio (assuming that means Ub/Us) approaches one (i.e. plug flow)? Is it entirely explained by the assumption of uniform A? It seems that A_b would be playing a key role here, as mentioned in lines 6-7. A_b influences the sliding speed in the Coulomb friction law, but the value of the flow-law coefficient that regulates creep closure is probably A in the model formulation (or is it A_b?).

Sliding ratio is Ub/Us. We fix figure 8C which had Us/Ub, and clarify this on page 14 with:
"and the sliding ratio *($\frac{U_b}{U_s}$)* for the linear sliding law"

We use the value of A for the momentum equations in the ice flow model. We use A_b in the subglacial hydrology model, and the Schoof sliding law. (This has been clarified in the text in response to a previous question)

This issue is independent of the subglacial hydrology simulation, since the linear sliding law inversion does not depend on the hydrology. However, we're uncertain why stiffer ice leads to better fits in our inversions. We suspect that the topology of the minimization problem is more complex with a higher A (due to increasing possibility of tradeoff between basal sliding and internal deformation), leading to the inversion finding a local minimums.

22.16-17: It would be compelling here if the authors could help the reader identify the effective pressures at which the behavioral transition in the sliding law occurs and relate them to the effective pressures shown in Fig 11b.

Comments from both reviews led us to scrutinize our explanation in greater detail. Previously we had done a simple calculation which showed that N was in the order of magnitude where the sliding law was in the Coulomb limit. However, when responding to the comments, we plotted the transition point for a range of N and U, and found that the Schoof sliding law was not in the Coulomb limit for the range of velocities and effective pressures in our domain.

Unfortunately, there was a discrepancy between the text and figure. While wrote in the text that the results were from \gamma_2=1e11, we had plotted the results of \gamma_2=1e09. The higher frequencies observed are not due to the sliding law, but because of a discrepancy in regularization. We have updated the figure with the results we intended to show, which are now similar to the other sliding laws.

Text has been updated as follows:

[Non-linear sliding laws subsection of Results] Page 18, 10-11 Lines + Page 21 Lines 1-3

~~"Figure (14 and 17) show the inversion results from the Weertman and Schoof sliding law respectively. Inverted basal drag using the Weertman sliding law is very similar to the results from the linear sliding law. In contrast, the inverted basal drag from the Schoof sliding law shows much higher frequency and magnitude spatial variations. This is reflected in the spatial distribution of the sliding ratio, with the Weertman sliding law resulting in a distribution similar to the linear sliding law, while the distribution from the Schoof sliding law shows much greater variation."~~

"Figure 5 shows the inversion results from the Budd and Schoof sliding laws. Inverted basal drag and the consequent sliding ratio using the two non-linear sliding laws are very similar to the results from the linear sliding law. Model mismatch is also similar for all three sliding laws (Figure 4)."

[Results Section] Page 22, Lines 7-19

~~"The pattern of basal drag inverted using the linear and Weertman sliding law show limited differences. This is due to the 10 fact that basal shear traction must satisfy the global stress balance (Joughin et al., 2004; Minchew et al., 2016). Both the linear and Weertman sliding law have the form τb = C · u1/m in the inversion, since effective pressure can be incorporated into the constant C for the Weertman sliding law. Previous work shows that in this case C ∝ u−1/m, and the recovered fields of basal drag are within a few percent of each other (Minchew et al., 2016). The basal drag and basal velocities from the the~~

~~linear sliding law to initiate the subglacial hydrology model are therefore self consistent with the subsequent inversion results of 15 the Weertman sliding law. The pattern of basal drag inverted using the Schoof sliding law however, shows both higher spatial variability and a higher magnitude of variability. This is a result of the Schoof sliding law shifting to Coulumb-like behaviour at low effective pressures."~~

"The pattern of basal drag inverted using the three different sliding laws show limited differences. This is due to the fact that basal shear traction must satisfy the global stress balance \citep{Joughin2004, Minchew2016}. The basal drag and basal velocities from the linear sliding law used to initiate the subglacial hydrology model are therefore self consistent with the subsequent inversion results of the two non-linear sliding laws. For the winter effective pressures predicted by the subglacial hydrology model, we find that the Schoof sliding law is in the viscous drag regime. For a representative basal velocity of 75 \unit{m yr^{-1}}, the transition to Coulomb friction occurs at effective pressures of approximately 0.7 MPa. This is below modelled effective pressures, which are above 1.3MPa for most of the study domain."

23. The conclusion that the modelled hydrology more resembles summer than winter conditions is not incorrect, but not especially meaningful. If the fragmentation of the drainage system is, in reality, what permits water storage in areas of high topography, then of course a continuum model fails to capture this effect. The authors acknowledge as much, but it diminishes the value of presenting this as a finding or conclusion of the study (as reported in the Abstract).

We feel it doesn't detract from the abstract, and showing this empirically makes it worth reporting. It may be a less relevant result for those with a strong theoretical background.

Technical corrections/queries (page.line):

1.13-14 "evolution of THE subglacial system"

Fixed

1.16-17: "result IN faster flow"

Fixed

2.10: AND missing

Fixed

2.13: "one" should be "some"

Fixed

5.1 "integrating" => "integrated"

Fixed

5.12: Looks like u_b should be \bar{u} in Eqn (17)

Fixed

8.4: "with respect to in the" too many words

Removed 'in'

14.3: "show" => "shown"

Deleted.

17.2: “the the”

Deleted.

19.Fig8c: Us/Ub? Sliding ratio sounds like it should be Ub/Us or Ub/Udef.

Fixed

25.5 “model output of the model”

Fixed

Incorporating modelled subglacial hydrology into inversions for basal drag

Conrad P. Koziol[1,2] and Neil Arnold[1]

[1]Scott Polar Research Institute, Cambridge U.K.
[2]now at the University of Edinburgh

Correspondence to: Conrad P. Koziol (ckoziol@gmail.com)

Abstract. A key challenge in modelling coupled ice flow - subglacial hydrology is initializing the state and parameters of the system. We address this problem by presenting a workflow for initializing these values at the start of a summer melt season. The workflow depends on running a subglacial hydrology model for the winter season, when the system is not forced by meltwater inputs, and ice velocities can be assumed constant. Key parameters of the winter run of the subglacial hydrology model are determined from an initial inversion for basal drag using a linear sliding law. The state of the subglacial hydrology model at the end of winter is incorporated into an inversion of basal drag using a non-linear sliding law which is a function of water pressure. We demonstrate this procedure in the Russell Glacier Area, and compare the output of the linear sliding law with two non-linear sliding laws. Additionally, we compare the ~~winter output of a recent subglacial hydrology model~~ modelled winter hydrological state to radar observations, and find that ~~the modelled state of the subglacial hydrology system at the end of winter~~ it is in line with summer rather than winter observations.

1 Introduction

Subglacial hydrology is an important control on ice velocities at the margin of the Greenland Ice Sheet. Observed seasonal acceleration of ice flow (Joughin et al., 2008; van de Wal et al., 2008; Zwally et al., 2002) is driven by the evolution of the subglacial system between distributed and channelized states in response to meltwater input (Bartholomew et al., 2010; Chandler et al., 2013; Cowton et al., 2013; Schoof, 2010). However, the impact of melt season intensity on seasonal and annual velocities, and how it may change in the future, is not fully understood. Observational studies of land-terminating sectors of the Greenland ice sheet reveal a complex set of possible interactions. Increased surface melt may result in faster flow early in the melt season, offset by a stronger late summer deceleration (Sundal et al., 2011). Increased runoff may also lead to more extensive drainage of the ice sheet base, reducing annual velocities due to slower winter flow (Sole et al., 2013). Long term observations in the ablation zone show surface melt and ice velocities are anti-correlated over decadal timescales (Stevens et al., 2016; Tedstone et al., 2015; van de Wal et al., 2015). The possible impact of surface melt on ice velocities at higher elevations is less well understood, as is the impact in marine-terminating sectors.

Recent subglacial hydrology models have progressed to simultaneously incorporating both distributed and efficient systems, explicitly treating the interaction between the two (de Fleurian et al., 2016; Hewitt, 2013; Pimentel et al., 2010; Schoof, 2010; Werder et al., 2013). These models have shown success in recreating the broad pattern of subglacial development in the summer melt-season inferred from GPS measurements (Bartholomew et al., 2011; van de Wal et al., 2015) and dye-tracing experiments (Chandler et al., 2013; Cowton et al., 2013). The development of the subglacial hydrological system has been shown to depend on feedbacks from ice velocities (Hoffman and Price, 2014). However, applications of recent hydrology models coupled with ice-flow models have been limited to idealized domains (Hewitt, 2013; Hoffman and Price, 2014; Hoffman et al., 2016; Pimentel and Flowers, 2010).

Initializing model parameters and state is necessary for applying a linked hydrology/ice dynamics model to the Greenland Ice Sheet. In contrast to the availability of measurements at the surface of ice sheets however, the conditions at the ice-bed interface are poorly constrained. Some key challenges for modelling are: the form of the sliding law which relates water pressures to basal drag; the values of the parameters in that relationship; and the values of water pressures at the ice-bed interface.

Inverse methods are an approach which can be used to constrain unknown variables or parameters in an ice sheet model. Inversions optimize the value of an unknown to minimize the discrepancy between model output and observed data. Since basal drag and the parameters of the sliding law are ~~one~~ some of the least constrained inputs to ice sheet models, a common application of inversions in glaciology is to determine the field of basal drag which best reproduces observed surface velocities. A variety of inversion methodologies have been applied in glaciology. These include iterative methods (Arthern et al., 2015), automatic differentiation (Goldberg and Heimbach, 2013; Heimbach and Bugnion, 2009; Martin and Monnier, 2014), and lagrangian multiplier methods based on control theory (MacAyeal, 1993; Morlighem et al., 2013).

In this study we develop an ice sheet model and inversion code which we apply to the Russell Glacier region of Western Greenland in order to invert for basal drag at the end of winter. The ice sheet model uses the hybrid formulation of Arthern et al. (2015) and Goldberg (2011) and is numerically similar to Arthern et al. (2015). The inversion procedure is based on automatic differentiation (Goldberg and Heimbach, 2013). Our application is novel in that we constrain the inversions using the output of a current subglacial hydrology model (Hewitt, 2013), and we investigate the impact of three different sliding laws (linear, ~~generalized Weertman~~ Budd, and Schoof-type (Hewitt, 2013)) on the patterns of basal drag predicted by the model. These developments form an important preliminary step towards a fully coupled model for ice dynamics and glacier hydrology which can be validated using current observational ice velocity data, and subsequently used for prognostic studies of possible future ice sheet responses to increased surface melt.

2 Methods

2.1 Hybrid Ice Sheet Model

2.1.1 Model Formulation

The ice sheet model implemented is based on the hybrid formulation described in Goldberg (2011) and Arthern et al. (2015), and uses the numerical implementation of Arthern et al. (2015).

Following Goldberg (2011) and Arthern et al. (2015), the conservation of momentum equations for depth-averaged velocities are:

$$\partial_x(4h\bar{\eta}\partial_x\bar{u} + 2h\bar{\eta}\partial_y\bar{v}) + \partial_y(h\bar{\eta}\partial_x\bar{v} + h\bar{\eta}\partial_y\bar{u}) - \tau_{bx} = \rho_i g h \partial_x s \tag{1}$$

$$\partial_y(4h\bar{\eta}\partial_y\bar{v} + 2h\bar{\eta}\partial_x\bar{u}) + \partial_x(h\bar{\eta}\partial_y\bar{u} + h\bar{\eta}\partial_x\bar{v}) - \tau_{by} = \rho_i g h \partial_y s \tag{2}$$

where $u(x,y,z)$ and $v(x,y,z)$ are velocities in the x and y directions, $\eta(x,y,z)$ is dynamic viscosity, $h(x,y)$ is ice thickness, $s(x,y)$ is surface elevation, $\tau_{bx(x,y)}$ and $\tau_{by}(x,y)$ are basal drag in the x and y directions, g is the magnitude of gravitational acceleration, and ρ_i is the density of ice. The overbar $(\bar{x})$ denotes the depth averaged value of a variable, so that $\bar{u}(x,y)$ and $\bar{v}(x,y)$ are depth averaged velocities and $\bar{\eta}(x,y)$ is depth averaged viscosity.

Basal drag is defined by the sliding law. Three different sliding laws are implemented in the ice sheet model:

$$\boldsymbol{\tau_b} = \beta^2 \boldsymbol{u_b} \tag{3}$$

$$\boldsymbol{\tau_b} = \mu_a N_+^p {U_b}^q \frac{\boldsymbol{u_b}}{U_b} \tag{4}$$

$$\boldsymbol{\tau_b} = \mu_b N_+ \left(\left(\frac{U_b}{U_b + \lambda_b A_b N_+^n} \right) \right)^{\frac{1}{n}} \frac{\boldsymbol{u_b}}{U_b} \tag{5}$$

where $\boldsymbol{\tau_b} = (\tau_{bx}(x,y), \tau_{by}(x,y))$ is the basal drag, $\boldsymbol{u_b} = (u_b, v_b) = (u(x,y,b), v(x,y,b))$ is the basal velocity, U_b is the sliding speed $(|\boldsymbol{u_b}|)$, $N(x,y) = \rho_i g h - p_w$ is the effective pressure at the ice sheet bed, p_w is water pressure, $\beta(x,y)$ is a basal drag coefficient, $\mu_a(x,y)$ is a drag coefficient, p and q are positive exponents, $\mu_b(x,y)$ is a limiting roughness slope, λ_b is the characteristic bed roughness length, and A_b and n are coefficients in Glen's flow law (Hewitt, 2013). A_b is the ice creep parameter ~~set to an appropriate value for basal ice .~~ used for basal ice. It set an order of magnitude lower than A to account for warmer ice at the base (following Hewitt (2013)). The value of A_b is used in both the Schoof sliding law, and in the subglacial hydrology model for determining creep closure of channels and cavities. The value of A is used in the momentum equations.

Following Hewitt (2013), negative effective pressures are eliminated by setting $N_+ = max(N, 0)$, and regularized with a small regularization constant.

The linear sliding law (Equation 3) represents all ice-bed interactions by a single friction coefficient β. The second and third equations are a ~~generalized Weertman~~ Budd sliding law and a Schoof sliding law respectively (Hewitt, 2013). These attempt to explicitly represent more complex interactions at the ice-bed-interface, in particular, the impact of basal water pressure.

Equation 4 is a power law commonly used in glaciology to describe basal rheology (e.g. Bueler and Brown, 2009; MacAyeal, 1989; Hewitt, 2013), although typically with no dependence on effective pressure ($p = 0$). At high effective pressures the Schoof sliding law has a similar form ($\cancel{\boldsymbol{\tau_b} \approx \mu_b(\lambda_b A_b)^{-1} U_b^{\frac{1}{n}}}$$\|\boldsymbol{\tau_b}\| \approx \mu_b(\lambda_b A_b)^{-1} U_b^{\frac{1}{n}}$), but transitions to a Coulomb description at low effective pressures ($\cancel{\boldsymbol{\tau_b} \approx \mu_b N}$$\|\boldsymbol{\tau_b}\| \approx \mu_b N$).

It is useful to represent the sliding laws in a common form:

$$\boldsymbol{\tau_b} = C\boldsymbol{u_b} \tag{6}$$

where C is a function multiplying basal velocities. The form and parameters of C depend on the sliding law.

The boundary conditions at the terminating margin of the ice sheet are:

$$2\bar{\eta}h(2\partial_x \bar{u} + \partial_y \bar{v})\hat{n}_x + \bar{\eta}h(\partial_y \bar{u} + \partial_x \bar{v})\hat{n}_y = \frac{g}{2}(\rho_i h^2 - \rho_w d^2)\hat{n}_x \tag{7}$$

$$2\bar{\eta}h(2\partial_y \bar{v} + \partial_x \bar{u})\hat{n}_y + \bar{\eta}h(\partial_y \bar{u} + \partial_x \bar{v})\hat{n}_x = \frac{g}{2}(\rho_i h^2 - \rho_w d^2)\hat{n}_y \tag{8}$$

where ρ_w is the density of water, d is the ice draft (zero at land terminating portions of the margin), and $\hat{n}_x$ and $\hat{n}_y$ are the components of the outward pointing unit vector normal to the terminating margin (Goldberg, 2011; Arthern et al., 2015).

Two further boundary conditions are used in the ice sheet model: a no-penetration condition at the margin of nunatuks, and a dirichlet boundary condition at the lateral margins of the ice sheet domain which are not the termination edge.

The equation for viscosity is:

$$\eta = \frac{1}{2}A^{\frac{-1}{n}}((\partial_x u)^2 + (\partial_y v)^2 + (\partial_x v)(\partial_y u) + (\partial_x v + \partial_y u)^2 + \frac{1}{4}(\partial_z u)^2 + \frac{1}{4}(\partial_z v)^2 + \epsilon_0)^{\frac{1-n}{2n}} \tag{9}$$

where ϵ_0 is a regularization term.Vertical shearing in the hybrid formulation is approximated by:

$$\partial_z u \approx \partial_z u + \partial_x w = \frac{\sigma_{xz}}{\eta}, \quad \partial_z v \approx \partial_z v + \partial_y w = \frac{\sigma_{yz}}{\eta} \tag{10}$$

As in Goldberg (2011) and Arthern et al. (2015), a linear relationship between vertical shear stresses and depth is assumed:

$$\sigma_{xz} = \tau_{bx}\frac{s-z}{h}, \quad \sigma_{yz} = \tau_{by}\frac{s-z}{h} \tag{11}$$

Viscosity is defined implicitly by Equation (9). With the standard choice of n=3, this is a cubic equation, and can be solved exactly. Alternatively, a previous value of viscosity can be used to calculate an updated value. This process can be iterated upon, to create a fixed point-iteration. The default procedure in the model is to do two iterations (Koziol, 2017).

The hybrid formulation of the conservation of momentum equations depend on depth integrated viscosity:

$$\bar{\eta} = \frac{1}{h}\int_{s}^{b} \eta dz \tag{12}$$

This integral, and others, are numerically ~~integrating~~ integrated using the Composite Simpson's Law.

Following Arthern et al. (2015), the following integral is defined:

$$F_a = \int_{s}^{b} \frac{1}{\eta}(\frac{s-z}{h})^a dz \tag{13}$$

This integral can be used to define expressions for surface velocity in terms of basal velocity, and basal velocity in terms of depth averaged velocity (Arthern et al., 2015):

$$\boldsymbol{u_s} = \boldsymbol{u_b}(1 + CF_1) \tag{14}$$

$$\bar{\boldsymbol{u}} = \boldsymbol{u_b}(1 + CF_2) \tag{15}$$

where F_1 and F_2 are determined using Equation 13 .

Additionally, defining C_{eff} as follows,

$$C_{eff} = \frac{C}{1 + CF_2} \tag{16}$$

leads to an expression for basal drag in terms of depth averaged velocity (Goldberg, 2011; Arthern et al., 2015):

$$\boldsymbol{\tau_b} = C_{eff}\bar{\boldsymbol{u}} \tag{17}$$

2.1.2 Model Implementation

As in Arthern et al. (2015), Equation 1 and 2 can be written in the following form:

$$\mathcal{L}(\bar{\boldsymbol{u}})\bar{\boldsymbol{u}} = \boldsymbol{f} \tag{18}$$

where:

$$\mathcal{L} = \begin{bmatrix} \partial_x 4h\bar{\eta}\partial_x + \partial_y 2h\bar{\eta}\partial_y - C_{eff} & \partial_x 2h\bar{\eta}\partial_y + \partial_y h\bar{\eta}\partial_x \\ \partial_y 2h\bar{\eta}\partial_x + \partial_x h\bar{\eta}\partial_y & \partial_y 4h\bar{\eta}\partial_y + \partial_x h\bar{\eta}\partial_x - C_{eff} \end{bmatrix} \tag{19}$$

and

$$\boldsymbol{f} = \begin{bmatrix} \rho_i g h \partial_x s \\ \rho_i g h \partial_y s \end{bmatrix} \tag{20}$$

Equation 18 is a non-linear equation for depth integrated velocity. The non-linearity arises since depth integrated viscosity is a function of velocity, and in the case of a non-linear sliding law, since C_{eff} is also a function of velocity. The ice sheet model solves Equation 18 on an Arakawa-C finite difference grid using a Picard iterative process.

Equation 18 is discretized following Arthern et al. (2015). The primary difference is that operators are appropriately extended to allow for periodic boundary conditions in the ISMIP-HOM experiments (Pattyn et al., 2008). Discretization of Equation 18 results in a linear system of equations, which can be written as:

$$\boldsymbol{L}\bar{\boldsymbol{x}} = \boldsymbol{b} \tag{21}$$

where the matrix ($\boldsymbol{L}$) corresponds to the operator $\mathcal{L}$, while the vector $\boldsymbol{x}$ corresponds to $\bar{\boldsymbol{u}}$, and the vector $\boldsymbol{b}$ corresponds to $\boldsymbol{f}$. Matlab's backslash operator is used to solve this system of equations. Alternatively, preconditioned iterative methods can be used (Arthern et al., 2015; Goldberg and Heimbach, 2013).

The Picard iteration linearizes Equation 18 by constructing $\boldsymbol{L}$ using the velocity of the previous iteration. An initial velocity guess and viscosity guess form the initial $\boldsymbol{L}$. Equation 18 is then solved for an updated velocity guess, which in turn can is used to update viscosity and C_{eff}. This process is repeated within a loop until the solution converges below a specified tolerance, or until a prescribed number of iterations are reached.

Evolution of surface-geometry is not included in the ice sheet model. This is appropriate since the ice-sheet model is applied on annual timescales, over which significant changes in ice sheet geometry are not expected.

The ice sheet model was tested against the ISMIP-HOM benchmark Experiments A and C (Pattyn et al., 2008), and found to compare favourably against previous models (Koziol, 2017).

2.2 Inversion Model

2.2.1 Model Formulation

This section describes the details of an inversion code developed in conjunction with the ice sheet model. The methodology is based on Goldberg and Heimbach (2013). However, the implementation developed here has a more limited capability due to software limitations.

The cost function returns a scalar which measures the fit of of the model to the observations. The cost function is defined as:

$$J = \gamma_1 \int\limits_{\Gamma_s} w \cdot (U_{obs} - U_s)^2 d\Gamma_s + \gamma_2 \int\limits_{\Gamma_b} (\nabla\alpha \cdot \nabla\alpha) d\Gamma_b \tag{22}$$

where γ_1 and γ_1 are user-defined scaling factors, Γ_s is the surface domain, Γ_b is the basal domain, $w(x,y)$ is a weighting function, $U_{obs}(x,y)$ are observed surface ice speeds, $U_s(x,y)$ are modelled surface speeds, and $\alpha(x,y)$ is the control parameter~~,~~.

The cost function defined above has two terms: $J = \gamma_1 J_0 + \gamma_2 J_{Reg}$. The first term ($J_0$) measures the weighted square of the difference between observed and modelled velocity. The second term (J_{Reg}) is a Tikhonov regularization term, which penalizes oscillations in α and stabilizes the inversion (Morlighem et al., 2013). Other formulations of the cost function are possible (e.g. Morlighem et al. (2013)).

The weighting function scales the mismatch between the observed and modelled surface velocities. It is used to incorporate a-priori knowledge about the quality of observations. Observations known to greater precision can be weighted higher, such that they have greater influence on the cost function than observations with a high error. The inverse of the variance of measurements is a statistically desirable weighting function.

The control parameter refers to the variable which the inversion process optimizes in order to best match model prediction and observations. Since our aim is to determine the basal drag, the control parameter is a parameter in the basal sliding law. For the linear sliding law, $\alpha = \beta^2$. For the ~~generalized Weertman~~ Budd sliding law, $\alpha = \mu_a$. Although the Schoof sliding law has two unknowns which can be inverted for, μ_b exerts a dominating control. Hence, λ_b is set to a constant while $\alpha = \mu_b$. In the numerical implementation of the adjoint, α is parameterized as ~~$\alpha(x,y) = exp(\zeta(x,y)$~~$\alpha(x,y) = exp(\zeta(x,y))$. This ensures that α remains positive, as expected for each of the three sliding laws. For simplicity, this is neglected in the remainder of the paper, and the discussion focuses on recovering α rather than ζ.

The inversion process aims to determine the field of α which minimizes the cost function. This is an optimization problem. Starting with an initial guess for α, the gradient of the cost function with respect to the initial input α ~~,~~is determined. The gradient provides a search direction for the optimization algorithm, which updates α. This process is repeated iteratively until α converges below a tolerance or until a maximum number of iterations occur. The critical component in this process is the gradient $\frac{dJ}{d\alpha}$. The process to calculate this gradient is described in the next two subsections.

2.2.2 Adjoint model description

The methodology to obtain the gradient $\frac{dJ}{d\alpha}$ follows from Goldberg and Heimbach (2013). The key concepts of this approach are first explained for a generic algorithm, before showing how they can be applied to the ice sheet model. This explanation follows that of Errico (1997) and Goldberg and Heimbach (2013).

Consider the model:

$$b = B(\boldsymbol{\phi}) \tag{23}$$

where ϕ is an arbitrary variable (or array of variables), and B can be considered a sequence of operations:

$$B(\boldsymbol{\phi}) = B_N((...(B_2(B_1(B_0(\boldsymbol{\phi}))))) \tag{24}$$

and each operation can be written as $b_N = B_N()$

Further, define a function J:

$$J = J(b) \tag{25}$$

where J returns a scalar. In the context of the adjoint model, the function is known as the cost function, objective function, or target function (Goldberg and Heimbach, 2013). This function quantifies an aspect of the model output which is of interest, such as the mean error of model output relative to observations.

The aim is to determine the gradient of the cost function J with respect to ~~in~~ the initial input ϕ. To provide context for the adjoint model, the tangent linear model (TLM) is presented first. In the TLM, a small perturbation in the input is propagated forward through the model to determine the corresponding perturbation in the output. Applying the chain rule to $J = J(b) = J(B(\phi))$ leads to the corresponding TLM:

$$\delta J = \left(\prod_{i=N}^{1} \frac{\partial b_i}{\partial b_{i-1}} \frac{\partial B_i}{\partial b_{i-1}} \right) \frac{\partial b_0}{\partial \phi_i} \frac{\partial B_0}{\partial \phi_i} \delta \phi_i \tag{26}$$

There are several observations about the TLM. First, the TLM determines the perturbation of δJ from the perturbation of a single element ϕ_i. As the perturbation $\delta\phi_i$ approaches zero, $\frac{\delta J}{\delta \phi_i}$ converges to $\frac{dJ}{d\phi_i}$. Second, to determine $\frac{dJ}{d\phi}$, the TLM needs to be run for each entry in ϕ. Although for small models this approach is feasible, the computational cost is too great for glaciological problems on domains of the size of interest. Finally, the TLM acts in a similar direction as the model B, in that the functions are applied successively starting with the counterpart to B_0 (Errico, 1997).

The concept behind the adjoint model is that rather than determining how changes in the input ϕ impact the cost function J, it can be more efficient to determine how changes in the cost function J impact the initial input ϕ. In the adjoint model, sensitivities of J are propagated backwards through the model, to determine the resulting change in ϕ. Similar to the TLM, the adjoint model is derived by applying the chain rule to $J = J(b) = J(B(\phi))$:

$$\frac{\partial J}{\partial \phi} = \left(\prod_{i=1}^{N} \left[\frac{\partial b_i}{\partial b_{i-1}} \frac{\partial B_i}{\partial B_{i-1}} \right]^T \right) \frac{\partial J}{\partial b_N} \tag{27}$$

Key observations about the adjoint model are: 1. In contrast to the TLM, which acts upon a perturbation, the adjoint model acts upon the sensitivity of the cost function. 2. A single run of the adjoint model is sufficient to determine the gradient $\frac{\delta J}{\delta \phi}$. 3. The adjoint model runs in reverse relative to both the model and the TLM, in that the adjoint model applies functions beginning with the counterpart to B_N and ending with the counterpart of B_0 (Errico, 1997).

2.2.3 Adjoint model implementation

The adjoint model is generated based on automatic differentiation (AD, Griewank and Walther (2008)) of the Matlab code implementations of the forward model. AD tools process an input code to generate a counterpart code which returns the corresponding gradient (or Jacobian). The central concept behind AD is that a computer program is fundamentally a sequence of elementary operations and functions. This admits the repeated application of the chain rule to generate a ~~derivate~~ derivative of high accuracy.

Multiple methodologies exist for AD tools to generate the ~~derivate~~ derivative code. Previous application of AD software to generate the adjoint in glaciology (Heimbach and Bugnion, 2009; Goldberg and Heimbach, 2013; Martin and Monnier, 2014) have used reverse accumulation AD tools (e.g. Giering et al., 2005; Hascoet and Pascual, 2004). These types of AD software are conceptually similar to the adjoint model. They are designed to determine the gradient of a function (input code) by propagating sensitivities of the output variables backwards to the input variables. Hence, an ice sheet model can be processed with relatively little modification by reverse accumulation AD tools to generate the adjoint model.

Here, we apply the open source AD tool ADiGator (Weinstein and Rao, 2011-2016), which in contrast to previous work is a forward accumulation AD tool. The methodology of forward accumulation is conceptually similar to the TLM. It is designed to determine the gradient of a function (input code) by propagating sensitivities of the input variables forward through the program to the output. Applying a forward AD tool to an ice sheet model to generate the adjoint is not feasible due to the size of the control space. Rather, we generate the adjoint by applying ADiGator to segments of the ice sheet model code, and multiplying the resulting Jacobians following Equation 27.

Pseudocode of the main ice sheet model routine is shown in Algorithm A1, and the corresponding code to calculate the adjoint is shown in Algorithm ~~2~~A2 (See Appendex),. Two new functions, S1 and S2 appear in the adjoint code. These encapsulate segments of code from the forward model and can be processed by ADiGator. The function S2 contains code which spans over two Picard iterations. The adjoint does not contain a for loop corresponding to iterating through the Picard iterations in reverse (c.f. Goldberg et al. (2016)). Rather, values from the final two Picard iterations of the forward model are saved and used as input for the adjoint code. The adjoint model is also modified to solve the cubic equation (following Arthern et al. (2015)) to determine η, rather than storing values from the previous iterations and implementing a fixed point iteration. This impacts the η, $\bar{\eta}$, and F_a functions, but leaves the overall structure the same. This is a necessary modification for ADiGator.

The adjoint code explicitly calculates several Jacobian matrices (lines 15 to 23 in Algorithm A2). ADiGator is applied to the corresponding functions to generate the Jacobian matrices, except the solution to the system of linear equations, which requires special treatment. A counterpart to the linear solve which returns the corresponding derivate is manually programmed following the procedure detailed in the appendix of Martin and Monnier (2014). The adjoint is then calculated by multiplying out the sensitivities of the cost function with the transposes of the Jacobian matrices. Although this process is more complicated and less flexible than previous approaches, it is necessary as no non-commercial AD reverse accumulation tool is available for Matlab.

This implementation of the adjoint is equivalent to previously published adjoint implementations (Goldberg and Heimbach, 2013; Martin and Monnier, 2014) restricted to one reverse step in the Picard iteration. This is mathematically equivalent to the Lagrangian Multiplier method introduced by MacAyeal (1993) (Heimbach and Bugnion, 2009).

The gradient from the adjoint model is used to solve the optimization problem which minimizes the cost function. The inversion code relies on minFunc (Schmidt, 2005), a publicly available Matlab unconstrained optimization package. The L-BFGS routine, with a Wolfe Condition backtracking line search, is applied in the inversion code. The cost function is discretized using the same finite difference operators as the ice sheet model.

Performance of the inversion code was verified using a series of identical twin-tests (Goldberg and Heimbach, 2013). Results are shown in Koziol (2017).

~~Ice sheet model main routine pseudocode~~

~~Pseudocode of the adjoint code~~

2.3 Subglacial Hydrology Model

This subglacial hydrology model used is described in detail in Hewitt (2013) and Banwell et al. (2016), and is similar conceptually to the model presented in Werder et al. (2013). Here, the version employed in Banwell et al. (2016) is applied.

Both distributed and channelized flow are represented in the subglacial hydrology model. Distributed flow is described by an average thickness and flux over a representative area. As in Banwell et al. (2016), the distributed system is composed ~~into~~ of two components: a cavity sheet, and an elastic sheet. The elastic sheet is included to simulate 'hydraulic jacking' from lake hydrofracture events, and is activated only when the effective pressure drops to zero and below. Channels have the potential to form along the edges and diagonals of the numerical grid. Channels are initiated by dissipative heating from the distributed system over an incipient channel width lengthscale. The model is written in Matlab, using a finite difference numerical grid, and an implicit forward time step method. For full details, consult Hewitt (2013) and Banwell et al. (2016).

2.4 Application to Russell Glacier Area

The Russell Glacier area is a land-terminating sector of the Greenland Ice Sheet (Figure 1). The ice sheet model and inversion code are applied to the Russell Glacier area to determine the basal boundary condition at the end of the winter season.

An outline of the study area is shown in (Figure 1). The northern and southern boundaries are selected to be roughly in line with basal watersheds determined using the Shreve (1972) approximation for hydraulic gradient. The northern boundary is approximately the same as used by Bougamont et al. (2014) and de Fleurian et al. (2016). The southern boundary is further south relative to Bougamont et al. (2014), but north of the southern boundary in de Fleurian et al. (2016). The eastern boundary was selected to extend up ice of the GPS stations (Tedstone and Neinow, 2017). The western boundary is the ice-margin. There is a nunatak near the western boundary.

The ice sheet model/inversion code are applied to determine the basal boundary condition at the end of the 2008-2009 winter season in the Russell Glacier study site. The end of the winter season is assumed to be day 120 of the year (April 30th).

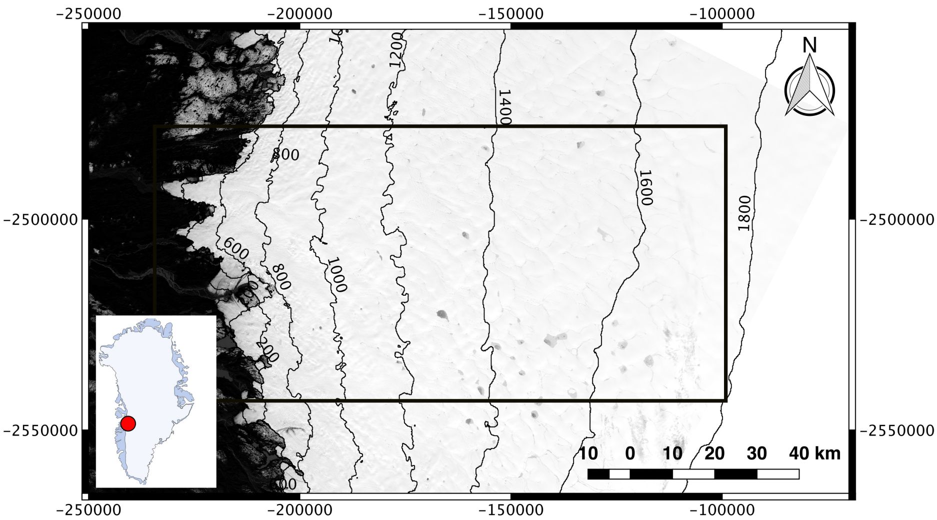

Figure 1. Landsat 8 satellite image, band 2, showing the Russell Glacier area. Black box outlines the study area. Inset shows the location in reference to Greenland.

Although the exact day is somewhat arbitrary, this day was selected as it is shortly before surface runoff begins in the study area, and shortly before GPS records in the study site show enhanced motion (Tedstone and Neinow, 2017).

Applying the ice sheet model/inversion code to the Russell Glacier area requires a number of datasets. Mean winter surface velocities for 2008/2009 (Figure ~~??~~2) are provided by the MEaSUREs Greenland Ice Sheet Velocity Map at 500 m resolution (Joughin et al., 2010a, b). Surface and basal topography (Figure ~~??~~2) are provided by the BedMachine2 dataset (Morlighem et al., 2014, 2015), and are resampled to 500 m resolution from 150 m resolution to match the velocity data. This is slightly coarser than the reported true resolution of 400 m for the ice thickness. The ~~500m~~ 500 m grid resolution results in a grid size of 132x274 for the domain. Fifty vertical layers are used for integration using Simpson's rule.

An important assumption made is that the mean winter velocities are representative of both the beginning and end of winter. This assumption is justified by observing published GPS records in Southwest Greenland (Colgan et al., 2012; van de Wal et al., 2015). These observations show that although velocities increase throughout the winter, the magnitude of the change is ~~relatively limited~~ limited (<25%).

Inversions are initialized using a basal drag set to the local driving stress smoothed by a 3x3 grid cell mean filter. The ice-margin boundary is described in the ice sheet model by Equation 7 and 8 while on the three other boundaries a Dirichlet boundary condition is applied. The inverse of the errors provided with the surface velocity measurements are used as weights in the cost function.

The results of inversions depends on the relative values of the scaling factors γ_1 to γ_2 in the cost function (Equation 22). For each sliding law, a series of inversions is performed with γ_1 set to 1 while varying γ_2. ~~A~~ An L-curve analysis is applied to select the inversion which best balances fitting the velocity observations while penalizing spurious oscillations in basal drag.

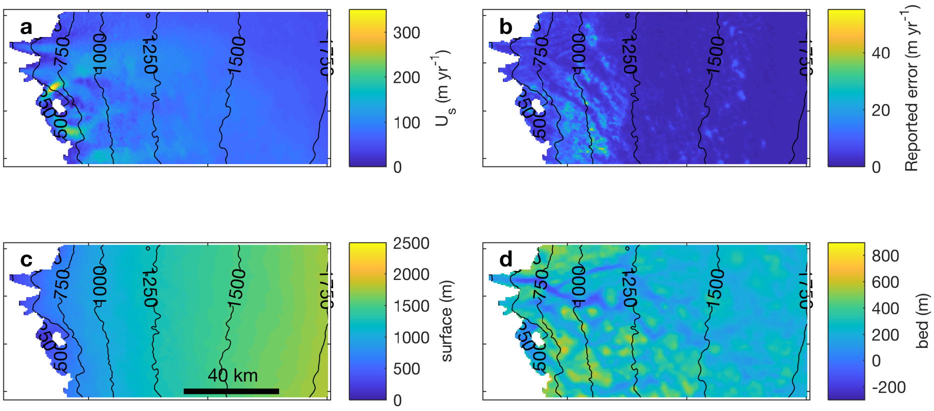

Figure 2. a) Velocity measurements from the MEaSUREs Greenland Ice Sheet Velocity Map at 500 m resolution for the Russell Glacier area (Joughin et al., 2010a, b). b) Reported error for the measurements. ~~a) Surface topography from~~ c) Surface topography from BedMachine2 ~~dataset (Morlighem et al., 2014, 2015) reinterpolated to~~ dataset (Morlighem et al., 2014, 2015) reinterpolated to 500 m~~. b) Basal topography at same resolution.~~. d) Basal topography at same resolution.

Parameters for the ice sheet model/inversion code are listed in Table 1. Similar to Hewitt (2013), the ice flow creep parameter (A) is selected to be $7 \cdot 10^{-25}$ $\mathrm{Pa}^3\mathrm{s}$. This corresponds to an ice temperature of approximately -7 °(Cuffey and Paterson, 2010). This choice for A results in the ratio of basal velocity to surface velocity remaining greater than 0.5 throughout the study area.

The parameters for the subglacial hydrology are the result of an extensive parameter search using a coupled ice-flow/subglacial hydrology model in (Koziol, 2017). Many of the parameters are the same as published in Banwell et al. (2016) and Hewitt (2013). However, testing of the reported optimal parameters for the Paakitsoq region reported by Banwell et al. (2016) using the integrated model showed poor agreement with GPS measurements due to insufficient volumes of water being evacuated from mid-elevations.

~~Flow chart showing the work flow for non-linear inversions~~

~~The workflow~~ A workflow is developed for incorporating modelled effective pressure into inversions using non-linear sliding laws~~is show in Figure ??~~. This workflow is motivated by the idea that both the subglacial hydrological system and ice flow are in quasi-steady state during the winter. This allows us to invert for background values of the constants in the sliding laws. The initial step is to invert using a linear sliding law for the basal drag coefficient. Basal velocities are calculated from modelled depth integrated velocities (Equation 15). The modelled basal drag and basal velocities then provide the necessary input for the subglacial hydrology model to calculate a distributed basal melt rate. The modelled distributed basal melt rate incorporates geothermal flux, but neglects heat loss to the interior of the ice sheet (Hewitt, 2013).

The subglacial hydrology model is then run for the winter season with the basal drag and basal velocities from the linear inversion. The model is run at ~~500m~~ 500 m resolution (identical to the inversions), with no-flow boundary conditions at the northern, southern, and eastern boundaries. The ice-margin is assumed to be at atmospheric pressure. This boundary condition

Symbol	Constant	Value	Units
A	Ice-flow parameter	$7 \cdot 10^{-25}$	$\mathrm{Pa^n s^{-1}}$
A_b	Ice-flow parameter for basal ice	$7 \cdot 10^{-24}$	$\mathrm{Pa^n s^{-1}}$
ρ_i	Ice density	917	$\mathrm{kgm^{-3}}$
g	Gravitational constant	9.81	$\mathrm{ms^{-2}}$
n	Exponent in Glen's flow law	3	
p	Exponent ~~generalized Weertman~~ in Budd sliding law	3^{-1}	
q	Exponent ~~generalized Weertman~~ in Budd sliding law	3^{-1}	
λ_b	bed roughness scale	1	m
t_y	Seconds per year	31536000	$\mathrm{syr^{-1}}$
ϵ	viscosity regularization parameter	$1 \cdot 10^{-14}$	$\mathrm{ms^{-1}}$

Table 1. Constants used in the ice sheet/inversion model applied to the Russell Glacier area.

is modified at necessary places to prevent inflow of water from beyond the ice sheet margin. Similarly to Banwell et al. (2016), the subglacial hydrology model is initialized with the thickness of the sheet flow layer set to 0.10 m. Testing showed that varying initial thickness has negligible impact. At this stage, the ice sheet model remains unconnected, and the input basal velocities are assumed to be constant. The subglacial hydrology model run provides a modelled water pressure distribution over the study site.

Finally, the non-linear inversions are run using the modelled water pressure from the subglacial hydrology model winter run. Two sets of inversions are conducted, one for the ~~generalized Weertman~~ Budd sliding law, and one for the Schoof sliding law. The first set of inversions seeks to determine the distribution of μ_a, while the second inverts for μ_b. Similar to the linear sliding law, an L-curve analysis is employed to determine the relative values of γ_1 to γ_2.

3 Results

3.1 Linear Inversion

Six inversions using the linear sliding law are run (Figure ~~??~~3). Using the L-curve plot, the inversion with $\gamma_2 = 1 \cdot 10^{-12}$ is selected as optimal. The value of J_0 for this inversion is $1.56 \cdot 10^{11}$.

~~The inversion converges in 46 iterations (Figure ??). The histogram of the the difference between observed and modelled velocities (Figure ??) has a maximum in the lowest bin, with a rapid decrease into a long tail. The maximum difference is approximately 165 . The difference between modelled and observed velocities is less than 10 for 88% of the cells in the study area, and less than 20 for 96% of the cells in the study area.~~ A map of the difference between observed and modelled velocities shows the highest difference occurs along the ice-margin and in the vicinity of the nunatak (Figure ~~??b~~4). Figure ~~??~~ 5 shows the inverted basal drag parameter, basal drag, and the sliding ratio $(\frac{U_b}{U_s})$ for the linear sliding law.

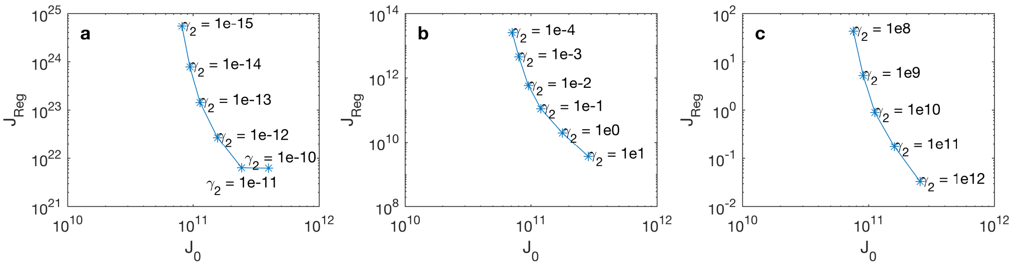

Figure 3. Log-log plot for L-curve analysis of inversions of the Russell Glacier area employing: a) linear sliding law. b) Budd slding law. c) Schoof sliding law.

~~Convergence~~

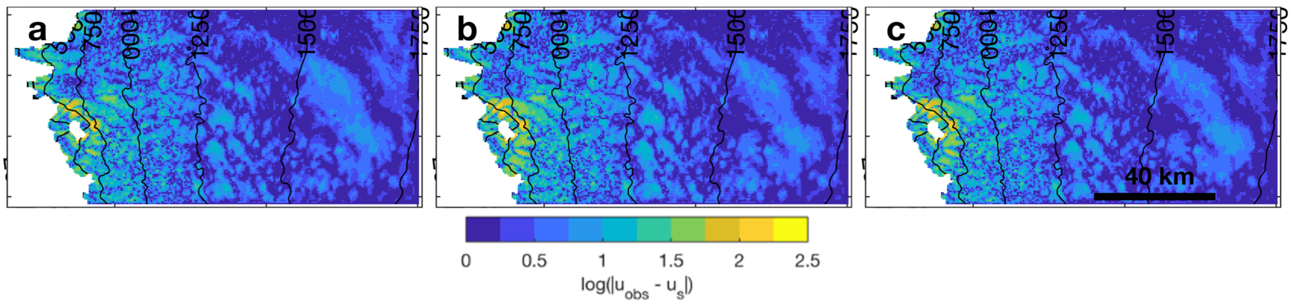

Figure 4. Map of the ~~optimization routine for~~ log of the ~~inversion~~ absolute difference between the observed and modelled surface velocities for inversions using: a~~linear~~) Linear sliding law, b) Budd sliding law, c) Schoof sliding law.

3.2 Subglacial Hydrology Model

Basal melt during the winter is shown in Figure 6. Most values are between 0.015 and 0.03 $\mathrm{m yr^{-1}}$, with higher values predominately occurring near the nunatak. The spatial pattern of melt broadly reflects the patterns of surface velocities (Figure ~~??~~2).

The subglacial hydrology model winter run evolves rapidly at the beginning of the run~~(Figure ??). By~~ . However, by day 50 of the model run ~~,~~the rate of change is significantly reduced~~. At~~ , and at by day 240 of the run the model is in an approximate steady state. ~~Relative to discharge at the base, changes in effective pressures have a much lower magnitude.~~

~~Plot showing the mean daily % change in water flux and effective pressure for a one year run.~~

The distribution of sheet thickness at the end of winter mirrors basal topography, with the sheet thickest in topographic lows (Figure 7). The maximum distributed system sheet thickness is 0.36 m~~, which is less than the bed roughness scale of 0.5~~ . The effective pressure also reflects the basal topography, with lowest effective pressures located in topographic lows. Since the lowest effective pressure is 0.44 MPa, no part of the ice sheet is near flotation. The model predicts minor channelization in two locations (not shown), with single channels extending from the margin several kilometres.

~~a) Histogram of the absolute difference between the observed and modelled surface velocities for the inversion using a linear sliding law. b) Map of the log of the absolute difference between the observed and modelled surface velocities for the same inversion.~~

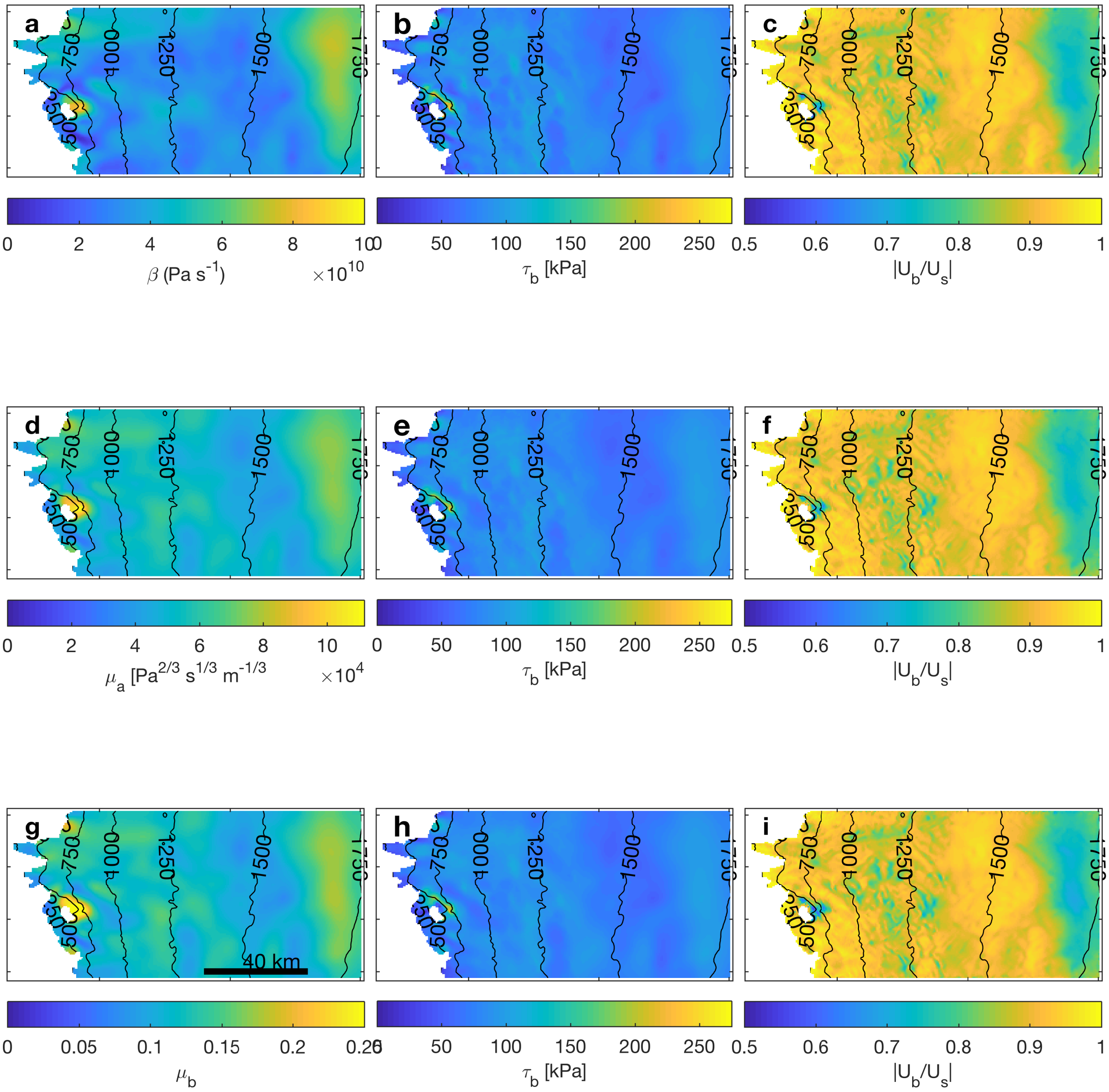

Figure 5.

Inversion results ~~using the linear sliding law. a) Inverted~~ for the three sliding laws. Subplots a-c relate to the Linear sliding law, d-f relate to the Budd sliding Law, and g-i relate to the Schoof sliding law. Subplots a,d, and h show the inverted drag parameter. ~~b) Basal drag. c) Sliding~~ Subplots b,e, and g show basal drag. Subplots c,f, and i show the sliding ratio.

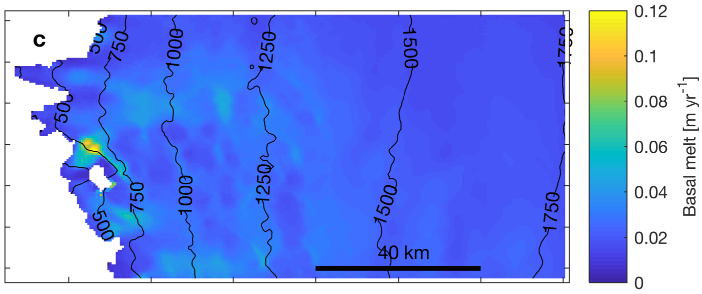

Figure 6. Modelled basal melt rate using basal velocities from linear inversion.

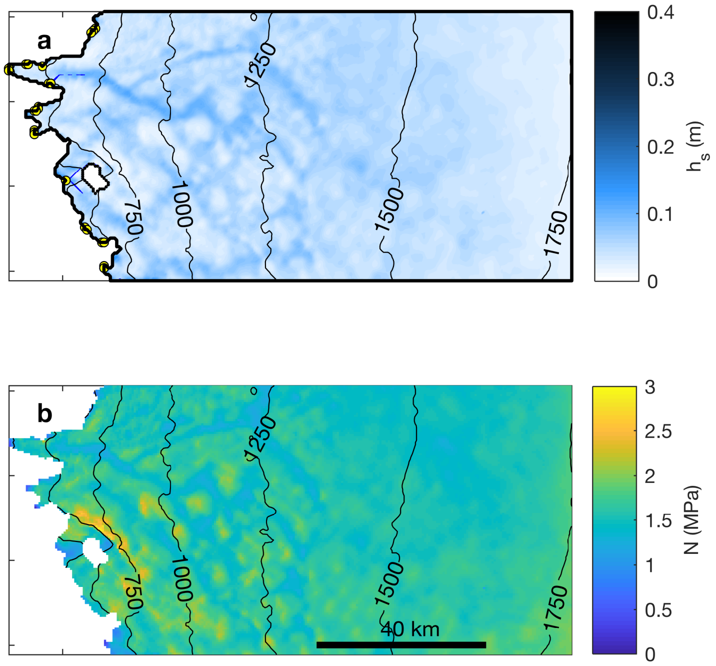

Figure 7. Modelled state of the subglacial hydrology system at the end of the winter. a) Map of sheet thickness, with black contours showing surface elevation. b) Map of effective pressure overlaid with surface elevation contours.

3.3 Non-linear sliding laws

An L-curve analysis (Figure ~~?? and ??~~3) is used to determine the optimum inversion for each of the non-linear sliding laws. The inversions corresponding to $\gamma_2 = 1$ is selected for the ~~Weertman~~ Budd sliding law, while the inversion corresponding to $\gamma_2 = 10^{11}$ is selected for the Schoof sliding law. These were selected so that the cost term of the inversions were similar to that of the linear sliding law. The two cost terms for the ~~Weertman~~ Budd and Schoof sliding laws are $J_0 = 1.78 \cdot 10^{11}$ and $J_0 = 1.60 \cdot 10^{11}$ respectively.

~~The histogram of the absolute difference between observed and modelled surface velocities for both non-linear sliding laws shows a similar distribution to the linear sliding law inversion (Figure ?? and ??). The Weertman sliding law results in a spatial distribution of misfit similar to the linear sliding law, while spatial distribution of error from the Schoof sliding law shows higher frequency variations. Model mismatch again is highest in the vicinity of the nunatak.~~

~~Figure (?? and ??) show the~~ Figure 5 shows the inversion results from the ~~Weertman~~ Budd and Schoof sliding ~~law respectively~~laws. Inverted basal drag ~~using the Weertman sliding law is~~ and the consequent sliding ratio using the two non-linear sliding laws are very similar to the results from the linear sliding law. ~~In contrast, the inverted basal drag from the Schoof sliding law shows much higher frequency and magnitude spatial variations. This is reflected in the spatial distribution of the sliding ratio, with the Weertman sliding law resulting in a distribution similar to the linear sliding law, while the distribution from the Schoof sliding law shows much greater variation.~~ Model mismatch is also similar for all three sliding laws (Figure 4).

~~Log-log plot for L-curve analysis of inversions of the Russell Glacier area employing generalized Weertman sliding law.~~

~~a) Histogram of the absolute difference between the observed and modelled surface velocities for the inversion using a generalized Weertman sliding law. b) Map of the log of the absolute difference between the observed and modelled surface velocities for the same inversion~~

~~Inversion results using the Weertman sliding law. a)Inverted drag parameter. b) Basal drag. c) Sliding ratio.~~

~~Log-log plot for L-curve analysis of inversions of the Russell Glacier area employing the Schoof sliding law.~~

~~a) Histogram of the absolute difference between the observed and modelled surface velocities for the inversion using a Schoof sliding law. b) Map of the log of the absolute difference between the observed and modelled surface velocities for the same inversion.~~

~~Inversion results using the Schoof sliding law. a) Inverted drag parameter. b) Basal drag. c) Sliding ratio.~~

4 Discussion

Inversions of the Russell Glacier area are run with a constant creep parameter A, corresponding to an ice temperature of approximately -7 °C (Cuffey and Paterson, 2010). For inversions with the linear sliding law, tests showed poorer results when A increased (corresponding to warmer ice). As A decreased, the sliding ratio approached one uniformly, and inversion results were better able to match observed surface velocities. The value of A was selected as a balance of model fit, while keeping a contribution to motion from internal deformation. Observations from two boreholes located in the Paakitsoq region show that internal deformation results in approximately 27-56% of ice velocities during winter (Ryser et al., 2014). In reality, A would have a heterogeneous distribution. By using a constant A, the basal drag parameter will account for some of the effects, which would otherwise be due to variation in A.

Basal velocities determined from the optimal inversion using a linear sliding law are input into the subglacial hydrology model. The distribution of basal velocities is used to both calculate the basal melt rate, and the cavity space in the continuum sheet flow. Due to the selection of a creep parameter such that the sliding ratio is relatively high, it is likely that basal velocities are overestimated. This would result in an overestimate of water generated at the ice-bed interface, and an overestimate of the capacity of cavity space. Application of a higher order ice sheet model would be advantageous in these regards.

The pattern of basal drag inverted using the ~~linear and Weertman sliding law~~ three different sliding laws show limited differences. This is due to the fact that basal shear traction must satisfy the global stress balance (Joughin et al., 2004; Minchew et al., 2016). ~~Both the linear and Weertman sliding law have the form~~ $\cancel{\tau_b = C \cdot u^{1/m}}$ ~~in the inversion, since effective pressure can be incorporated into the constant C for the Weertman sliding law. Previous work shows that in this case~~ $\cancel{C \propto u^{-1/m}}$~~, and the recovered fields of basal drag are within a few percent of each other (Minchew et al., 2016).~~ The basal drag and basal velocities from the ~~the~~ linear sliding law used to initiate the subglacial hydrology model are therefore self consistent with the subsequent inversion results of the ~~Weertman sliding law. The pattern of basal drag inverted using the~~ two non-linear sliding laws. For the winter effective pressures predicted by the subglacial hydrology model, we find that the Schoof sliding law ~~however, shows both higher spatial variability and a higher magnitude of variability. This is a result of the Schoof sliding law shifting to Coulumb-like behaviour at low effective pressures .~~ is in the viscous drag regime. For a representative basal velocity of 75 $\mathrm{m\,yr^{-1}}$, the transition to Coulomb friction occurs at effective pressures of approximately 0.7 MPa. This is below modelled effective pressures, which are above 1.3MPa for most of the study domain.

Interpretation of radar lines in the Russell Glacier area suggests significant winter storage of water along topographic highs, while significant water flow through topographic lows occurs during the summer melt seasons (Chu et al., 2016). Based on these observations, the subglacial hydrology runs are ~~is~~ reflective of summer conditions rather than winter conditions. Water storage, which would be characterized by high sheet thickness, is not observed along topographic highs. Chu et al. (2016) attribute storage on topographic ridges to water storage in parts of the distributed system which become isolated at the end of the melt season. In contrast, porous sediments in bedrock troughs are hypothesized to allow water to drain (Chu et al., 2016). The treatment of the bed in the subglacial hydrology model is uniform. It does not account for differences in till cover or bed properties, nor does it account for sub-grid scale heterogeneity in the distributed system, which is likely the cause of water storage. Replicating these observations likely requires the implementation of another model component, such as the weakly connected distributed system proposed by Hoffman et al. (2016). In general, model output from the subglacial hydrology model can be expected to be much more sensitive to the model formulation during the winter than the summer, when the system is forced by high water input. Inline with inferences from tracer injections (Chandler et al., 2013), the model does not predict a channelized system at the margin during the winter.

The initialization procedure introduced is not capable of producing the inferred year on year differences in the subglacial hydrological system at the end of winter. Currently, the subglacial hydrology reaches an approximate steady state by day 240, and is not particularly sensitive to the initialization of the distributed sheet thickness. A full steady state takes approximately two years (Hewitt, 2013). In contrast, observations suggest that summer melt has an impact on the state of the hydrological system during the subsequent winter (Chu et al., 2016; Sole et al., 2013). The model output ~~of the model~~ therefore can only be considered an approximation to a generic hydrological state. Any discrepancy between the modelled and actual hydrological system is expected to have a greater impact on inversions using the Schoof sliding law, since it has a stronger dependence on effective pressure. In the limit of viscous flow, the Schoof sliding law depends on N. In contrast, the ~~generalized Weertman~~ Budd law is a function of $N^{1/3}$ (Budd et al., 1979). All inversions are conducted using mean winter velocities from 2008-2009. Annual differences in mean winter velocities are expected to have a minimal impact, as observed year on year differences are on the order 20 myr^{-1}, which is not significantly greater than the velocity mismatch in the inversions.

Other procedures for determining the background parameters of sliding laws can likely be devised. Currently the procedure only uses mean winter velocities. Using mean annual velocities may improve estimates of the sliding law parameters by incorporating information from the melt season. A subglacial hydrological model could be run for an entire year, and basal parameters determined from an annual average water pressure. A key difficulty is running the hydrological model during the summer, as the development of the system is known to depend on feedbacks with velocity (Hoffman and Price, 2014). This issue can be avoided by using velocity measurements from remote-sensing as a model forcing (e.g Fahnestock et al., 2016). An advantage of running the subglacial hydrology model during the summer months is that model output may be more representative of water flow beneath the ice sheet. Although in its current form the model is too complex, a simplified subglacial hydrology model may be suitable to time dependent adjoint modelling (Goldberg and Heimbach, 2013). Here, we have assumed that the parameters of the sliding law are time independent. This assumption is better suited for bedrock than till, as properties of till are dependent on saturation and deformational history (Minchew et al., 2016).

5 Conclusions

A new ice sheet model and adjoint code are presented. The ice sheet model is coupled to a recent subglacial hydrology model (Hewitt, 2013). A procedure for initializing a coupled subglacial hydrology/ice sheet model using a winter run is also proposed. The modelled state of the subglacial hydrological system at the end of winter appears to reflect summer observations rather than winter observations. This is likely the result of model formulation rather than the initialization procedure, and ~~the initialization procedure should~~ could lend support to the potential need for an additional, weakly connected component in hydrological models (Hoffman et al 2016). However, the initialization procedure presented here will continue to prove useful as model development advances, as this is independent of the hydrological model used. The results are subsequently used to run inversions using non-linear sliding laws which are functions of effective pressure. This allows the background parameters for the sliding law to be determined. To date, this appears to be the first work to incorporate modelled water pressures in an inversion, and the first to invert with a sliding law explicitly dependent on effective pressure. The usefulness of this inversion for initiating coupled ice sheet/ hydrology model simulations is shown in an upcoming publication.

Code and data availability. All datasets used are publicly available. Code is currently not available.

Competing interests. The authors declare that they have no conflict of interest.

Acknowledgements. We would like to thank ~~the~~ M. Morlighem and I. Joughin for the BedMachine2 and MEaSUREs datasets, and I. Hewitt for generously sharing the subglacial hydrology code. C.P. Koziol would like to acknowledge R. Arthern for guidance on writing an ice sheet model and inversion code, as well as B. Minchew, P. Christoffersen, and D. Goldberg for thoughtful discussions. C.P. Koziol was funded through St. John's College, Cambridge and (in part) by NERC standard grant NE/M003590/1.

Appendix A: Appendix A

Algorithm 1 Ice sheet model main routine pseudocode

Initialize: $\bar{u}$, η, C, C_{eff}, α %From Shallow Ice Approximation
for $j = 1, 2, 3, ..., N$ %Picard Iterations
$\eta = \boldsymbol{\eta}(\bar{u}, \eta, C_{eff})$ %Viscosity (Eq. 9)
$\bar{\eta} = \bar{\boldsymbol{\eta}}(\eta)$ %Depth integrated Viscosity (Eq. 20)
$F_2 = \boldsymbol{F_a}(\eta, a = 2)$ %F-integral (Eq. 13)
$C = \boldsymbol{C}(\bar{u}, \alpha, C, F2)$ %Basal drag parameter (Eq. 6)
$C_{eff} = \boldsymbol{C_{eff}}(C, F2)$ %Effective basal drag parameter (Eq. 16)
$\bar{u} = \boldsymbol{u}(C_{eff}, \bar{\eta})$ %Velocities (Eq. 21)
end
$J = \boldsymbol{J}(\bar{u}, C_{eff}, \alpha)$ %Cost Function Eq. 27

Algorithm 2 Pseudocode of the adjoint code

% Encapsulate segments of code into functions
function S1$(\bar{u}, \alpha, C, F2)$
$C = \boldsymbol{C}(\bar{u}, \alpha, C, F2)$
$C_{eff} = \boldsymbol{C_{eff}}(C, F2)$
return C_{eff}

function S2$(\bar{u}, \alpha, C, F2)$
$C = \boldsymbol{C}(\bar{u}, \alpha, C, F2)$
$C_{eff} = \boldsymbol{C_{eff}}(C, F2)$
$\eta = \boldsymbol{\eta}(\bar{u}, C_{eff})$
$\bar{\eta} = \bar{\boldsymbol{\eta}}(\eta)$
return $\bar{\eta}$

% Calculate Jacobian matrices ($\mathrm{D}f|_p = \frac{\partial f_i}{\partial p_j}$)
$\mathrm{D}J|_{\bar{u}}$ = **ADiGator(*J***, $\bar{u}^N$, C_{eff}^N, α)
$\mathrm{D}J|_{C_{eff}}$ = **ADiGator(*J***, $\bar{u}^N$, C_{eff}^N, α)
$\mathrm{D}J|_{\alpha}$ = **ADiGator(*J***, $\bar{u}^N$, C_{eff}^N, α)

$\mathrm{D}S1|_{\alpha}$= **ADiGator(S1**, $\bar{u}^{N-1}$, α, C^{N-1}, F_2^N)
$\mathrm{D}S2|_{\alpha}$= **ADiGator(S2**, $\bar{u}^{N-1}$, α, C^{N-2}, F_2^{N-1})

% The Jacobian of the velocity solve is calculated using a manually programmed function
$\mathrm{D}u|_{C_{eff}}$= **U_jac(** $\bar{u}^N$, C_{eff}^N, $\bar{\eta}$)
$\mathrm{D}u|_{\bar{\eta}}$ = **U_jac(** $\bar{u}^N$, C_{eff}^N, $\bar{\eta}$)

% The adjoint (Eq. 27)
$\frac{dJ}{d\alpha} = (\mathrm{D}S1|_{\alpha})^T (\mathrm{D}\bar{u}|_{C_{eff}})^T (\mathrm{D}J|_{\bar{u}}) +$
$\qquad (\mathrm{D}S2|_{\alpha})^T (\mathrm{D}\bar{u}|_{\bar{\eta}})^T (\mathrm{D}J|_{\bar{u}}) +$
$\qquad (\mathrm{D}S1|_{\alpha})^T (\mathrm{D}J|_{C_{eff}}) + \mathrm{D}J|_{\alpha}$

References

Arthern, R. J., Hindmarsh, R. C. A., and Williams, C. R.: Flow speed within the Antarctic ice sheet and its controls inferred from satellite observations, Journal of Geophysical Research: Earth Surface, 120, 1171–1188, https://doi.org/10.1002/2014JF003239, http://doi.wiley.com/10.1002/2014JF003239, 2015.

Banwell, A., Hewitt, I., Willis, I., and Arnold, N.: Moulin density controls drainage development beneath the Greenland Ice Sheet, Journal of Geophysical Research: Earth Surface, https://doi.org/10.1002/2015JF003801, http://doi.wiley.com/10.1002/2015JF003801, 2016.

Bartholomew, I., Nienow, P., Mair, D., Hubbard, A., King, M. A., and Sole, A.: Seasonal evolution of subglacial drainage and acceleration in a Greenland outlet glacier, Nature Geoscience, 3, 408–411, https://doi.org/10.1038/ngeo863, http://www.nature.com/doifinder/10.1038/ngeo863, 2010.

Bartholomew, I., Nienow, P., Sole, A., Mair, D., Cowton, T., Palmer, S., and Wadham, J.: Supraglacial forcing of subglacial drainage in the ablation zone of the Greenland ice sheet, Geophysical Research Letters, 38, n/a–n/a, https://doi.org/10.1029/2011GL047063, http://doi.wiley.com/10.1029/2011GL047063, 2011.

Bougamont, M., Christoffersen, P., A L, H., Fitzpatrick, A., Doyle, S., and Carter, S.: Sensitive response of the Greenland Ice Sheet to surface melt drainage over a soft bed, Nature communications, 5, 2014.

Budd, W., Keage, P., and Blundy, N.: Empirical studies of ice sliding, Journal of glaciology, 23, 157–170, 1979.

Bueler, E. and Brown, J.: Shallow shelf approximation as a "sliding law" in a thermomechanically coupled ice sheet model, Journal of Geophysical Research, 114, F03 008, https://doi.org/10.1029/2008JF001179, http://doi.wiley.com/10.1029/2008JF001179, 2009.

Chandler, D. M., Wadham, J. L., Lis, G. P., Cowton, T., Sole, A., Bartholomew, I., Telling, J., Nienow, P., Bagshaw, E. B., Mair, D., Vinen, S., and Hubbard, A.: Evolution of the subglacial drainage system beneath the Greenland Ice Sheet revealed by tracers, Nature Geoscience, 6, 195–198, https://doi.org/10.1038/ngeo1737, http://www.nature.com/doifinder/10.1038/ngeo1737, 2013.

Chu, W., Schroeder, D. M., Seroussi, H., Creyts, T. T., Palmer, S. J., and Bell, R. E.: Extensive winter subglacial water storage beneath the Greenland Ice Sheet, Geophysical Research Letters, pp. 484–492, https://doi.org/10.1002/2016GL071538, http://doi.wiley.com/10.1002/2016GL071538, 2016.

Colgan, W., Rajaram, H., Anderson, R., Steffen, K., Zwally, J., Phillips, T., and Abdalati, W.: The annual glaciohydrology cycle in the ablation zone of the Greenland ice sheet: Part 2. Observed and modeled ice flow, Journal of Glaciology, 58, 51–64, https://doi.org/10.3189/2012JoG11J081, http://www.igsoc.org/journal/current/207/j11J081.pdf, 2012.

Cowton, T., Nienow, P., Sole, A., Wadham, J., Lis, G., Bartholomew, I., Mair, D., and Chandler, D.: Evolution of drainage system morphology at a land-terminating Greenlandic outlet glacier, Journal of Geophysical Research: Earth Surface, 118, 29–41, https://doi.org/10.1029/2012JF002540, http://doi.wiley.com/10.1029/2012JF002540, 2013.

Cuffey, K. and Paterson, W.: The physics of glaciers, Academic Press, 2010.

de Fleurian, B., Morlighem, M., Seroussi, H., Rignot, E., van den Broeke, M. R., Munneke, P. K., Mouginot, J., Smeets, P. C. J. P., and Tedstone, A. J.: A modeling study of the effect of runoff variability on the effective pressure beneath Russell Glacier, West Greenland, Journal of Geophysical Research: Earth Surface, https://doi.org/10.1002/2016JF003842, http://doi.wiley.com/10.1002/2016JF003842, 2016.

Errico, R. M.: What is an Adjoint?, Bulletin of the American Meteorological Society, 78, 2577–2591, https://doi.org/10.1175/1520-0477(1997)078<2577:WIAAM>2.0.CO;2, 1997.

Fahnestock, M., Scambos, T., Moon, T., Gardner, A., Haran, T., and Klinger, M.: Rapid large-area mapping of ice flow using Landsat 8, Remote Sensing of Environment, 185, 84–94, https://doi.org/10.1016/j.rse.2015.11.023, http://dx.doi.org/10.1016/j.rse.2015.11.023, 2016.

Giering, R., Kaminski, T., and Slawig, T.: Generating Efficient Derivative Code with TAF Adjoint and Tangent Linear Euler Flow Around an Airfoil, Future Gener. Comput. Syst., 21, 1345–1355, https://doi.org/10.1016/j.future.2004.11.003, http://dx.doi.org/10.1016/j.future.2004.11.003, 2005.

Goldberg, D. N.: A variationally derived, depth-integrated approximation to a higher-order glaciological flow model, Journal of Glaciology, 57, 157–170, https://doi.org/10.3189/002214311795306763, 2011.

Goldberg, D. N. and Heimbach, P.: Parameter and state estimation with a time-dependent adjoint marine ice sheet model, The Cryosphere, 7, 1659–1678, https://doi.org/10.5194/tc-7-1659-2013, http://www.the-cryosphere.net/7/1659/2013/, 2013.

Goldberg, D. N., Narayanan, S. H. K., Hascoet, L., and Utke, J.: An optimized treatment for algorithmic differentiation of an important glaciological fixed-point problem, Geoscientific Model Development, 9, 1891–1904, https://doi.org/10.5194/gmd-9-1891-2016, 2016.

Griewank, A. and Walther, A.: Evaluating derivatives: principles and techniques of algorithmic differentiation, SIAM, 2008.

Hascoet, L. and Pascual, V.: TAPENADE 2.1 users guide, http://www-tapenade.inria.fr:8080/tapenade/index.jsp, 2004.

Heimbach, P. and Bugnion, V.: Greenland ice-sheet volume sensitivity to basal, surface and initial conditions derived from an adjoint model, Annals of Glaciology, 50, 67–80, https://doi.org/10.3189/172756409789624256, 2009.

Hewitt, I.: Seasonal changes in ice sheet motion due to melt water lubrication, Earth and Planetary Science Letters, 371-372, 16–25, https://doi.org/10.1016/j.epsl.2013.04.022, http://linkinghub.elsevier.com/retrieve/pii/S0012821X13002045, 2013.

Hoffman, M. and Price, S.: Feedbacks between coupled subglacial hydrology and glacier dynamics, Journal of Geophysical Research: Earth Surface, 119, 414–436, https://doi.org/10.1002/2013JF002943, 2014.

Hoffman, M. J., Andrews, L. C., Price, S. A., Catania, G. A., Neumann, T. A., Luethi, M. P., Gulley, J., Ryser, C., Hawley, R. L., and Morriss, B. F.: Greenland subglacial drainage evolution regulated by weakly-connected regions of the bed, Nature Communications, https://doi.org/10.1038/ncomms13903, 2016.

Joughin, I., MacAyeal, D. R., and Tulaczyk, S.: Basal shear stress of the Ross ice streams from control method inversions, Journal of Geophysical Research B: Solid Earth, 109, 1–20, https://doi.org/10.1029/2003JB002960, 2004.

Joughin, I., Das, S. B., King, M. A., Smith, B. E., Howat, I. M., and Moon, T.: Seasonal speedup along the western flank of the Greenland Ice Sheet., Science (New York, N.Y.), 320, 781–3, https://doi.org/10.1126/science.1153288, http://www.sciencemag.org/cgi/doi/10.1126/science.1153288http://www.ncbi.nlm.nih.gov/pubmed/18420901, 2008.

Joughin, I., Smith, B. E., Howat, I. M., Scambos, T., and Moon, T.: Greenland flow variability from ice-sheet-wide velocity mapping, Journal of Glaciology, 56, 415–430, https://doi.org/10.3189/002214310792447734, 2010a.

Joughin, I., Smith, B. E., Howat, I. M., Scambos, T., and Moon, T.: MEaSUREs Greenland Ice Velocity Map from InSAR Data. Boulder, Colorado, USA: NASA DAAC at the National Snow and Ice Data Center., https://doi.org/10.5067/MEASURES/CRYOSPHERE/nsidc-0478.001, 2010b.

Koziol, C. P.: Modelling the impact of surface melt on the hydrology and dynamics of the Greenland Ice Sheet, Ph.D. thesis, University of Cambridge, 2017.

MacAyeal, D.: A tutorial on the use of control methods in ice sheet modeling, J. Glaciol, 39, 91–98, https://doi.org/10.1017/S0022143000015744, 1993.

MacAyeal, D. R.: Large-scale ice flow over a viscous basal sediment: Theory and application to ice stream B, Antarctica, Journal of Geophysical Research: Solid Earth, 94, 4071–4087, https://doi.org/10.1029/JB094iB04p04071, 1989.

Martin, N. and Monnier, J.: Adjoint accuracy for the full Stokes ice flow model: limits to the transmission of basal friction variability to the surface, The Cryosphere, 8, 721–741, https://doi.org/10.5194/tc-8-721-2014, http://www.the-cryosphere.net/8/721/2014/, 2014.

Minchew, B., Simons, M., Bjornsson, H., Palsson, F., Morlighem, M., Seroussi, H., Larour, E., and Hensley, S.: Plastic bed beneath Hofsjokull ice cap, central Iceland, and the sensitivity of ice flow to surface meltwater flux, Journal of Glaciology, 62, 147–158, https://doi.org/10.1017/jog.2016.26, 2016.

Morlighem, M., Seroussi, H., Larour, E., and Rignot, E.: Inversion of basal friction in Antarctica using exact and incomplete adjoints of a higher-order model, Journal of Geophysical Research: Earth Surface, 118, 1746–1753, https://doi.org/10.1002/jgrf.20125, 2013.

Morlighem, M., Rignot, E., Mouginot, J., Seroussi, H., and Larour, E.: Deeply incised submarine glacial valleys beneath the Greenland ice sheet, Nature Geoscience, 7, 418–422, https://doi.org/10.1038/ngeo2167, http://www.nature.com/doifinder/10.1038/ngeo2167, 2014.

Morlighem, M., Rignot, E., Mouginot, J., Seroussi, H., and Larour, E.: IceBridge BedMachine Greenland, Version 2, Thickness. Boulder, Colorado USA: NASA DAAC at the National Snow and Ice Data Center., https://doi.org/10.5067/AD7B0HQNSJ29, 2015.

Pattyn, F., Perichon, L., Aschwanden, A., Breuer, B., De Smedt, B., Gagliardini, O., Gudmundsson, G. H., Hindmarsh, R. C. A., Hubbard, A., Johnson, J. V., Kleiner, T., Konovalov, Y., Martin, C., and Payne, A. J.: Benchmark experiments for higher-order and full-Stokes ice sheet models (ISMIP–HOM) *, The Cryosphere, 2, 95–108, https://doi.org/10.5194/tcd-2-111-2008, www.the-cryosphere.net/2/95/2008/{%}5Cnhttp://homepages.ulb.ac.be/, 2008.

Pimentel, S. and Flowers, G. E.: A numerical study of hydrologically driven glacier dynamics and subglacial flooding, Proceedings of the Royal Society of London A: Mathematical, Physical and Engineering Sciences, 467, 537–558, https://doi.org/10.1098/rspa.2010.0211, http://rspa.royalsocietypublishing.org/content/467/2126/537, 2010.

Pimentel, S., Flowers, G. E., and Schoof, C. G.: A hydrologically coupled higher-order flow-band model of ice dynamics with a Coulomb friction sliding law, Journal of Geophysical Research, 115, F04 023, https://doi.org/10.1029/2009JF001621, http://doi.wiley.com/10.1029/2009JF001621, 2010.

Ryser, C., Luthi, M. P., Andrews, L. C., Hoffman, M. J., Catania, G. A., Hawley, R. L., Neumann, T. A., and Kristensen, S. S.: Sustained high basal motion of the Greenland ice sheet revealed by borehole deformation, Journal of Glaciology, 60, 647–660, https://doi.org/10.3189/2014JoG13J196, 2014.

Schmidt, M.: minFunc: unconstrained differentiable multivariate optimization in Matlab, http://www.cs.ubc.ca/~schmidtm/Software/minFunc.html, 2005.

Schoof, C.: Ice-sheet acceleration driven by melt supply variability., Nature, 468, 803–6, https://doi.org/10.1038/nature09618, http://www.nature.com/doifinder/10.1038/nature09618http://www.ncbi.nlm.nih.gov/pubmed/21150994, 2010.

Shreve, R.: The Movement of Water in Glaciers, Journal of Glaciology, 11, 1972.

Sole, A., Nienow, P., Bartholomew, I., Mair, D., Cowton, T., Tedstone, A., and King, M. A.: Winter motion mediates dynamic response of the Greenland Ice Sheet to warmer summers, Geophysical Research Letters, 40, 3940–3944, https://doi.org/10.1002/grl.50764, http://doi.wiley.com/10.1002/grl.50764, 2013.

Stevens, L. A., Behn, M. D., Das, S. B., Joughin, I., Noel, B. P. Y., van den Broeke, M. R., and Herring, T.: Greenland Ice Sheet flow response to runoff variability, Geophysical Research Letters, 43, 11,295–11,303, https://doi.org/10.1002/2016GL070414, http://dx.doi.org/10.1002/2016GL070414, 2016GL070414, 2016.

Sundal, A. V., Shepherd, A., Nienow, P., Hanna, E., Palmer, S., and Huybrechts, P.: Melt-induced speed-up of Greenland ice sheet offset by efficient subglacial drainage., Nature, 469, 521–4, https://doi.org/10.1038/nature09740, http://www.nature.com/doifinder/10.1038/nature09740http://www.ncbi.nlm.nih.gov/pubmed/21270891, 2011.

Tedstone, A. and Neinow, P.: Ice motion measurements, south-west Greenland Ice Sheet, https://data.bas.ac.uk/metadata.php?id=GB/NERC/BAS/PDC/00841, https://doi.org/http://doi.org/b2f3, nERC, Polar Data Centre, 2017.

Tedstone, A. J., Nienow, P. W., Gourmelen, N., Dehecq, A., Goldberg, D., and Hanna, E.: Decadal slowdown of a land-terminating sector of the Greenland Ice Sheet despite warming, Nature, 526, 692–695, https://doi.org/10.1038/nature15722, http://www.nature.com/doifinder/10.1038/nature15722, 2015.

van de Wal, R. S. W., Boot, W., van den Broeke, M. R., Smeets, C. J. P. P., Reijmer, C. H., Donker, J. J. A., and Oerlemans, J.: Large and rapid melt-induced velocity changes in the ablation zone of the Greenland Ice Sheet., Science (New York, N.Y.), 321, 111–3, https://doi.org/10.1126/science.1158540, http://www.sciencemag.org/cgi/doi/10.1126/science.1158540http://www.ncbi.nlm.nih.gov/pubmed/18599784, 2008.

van de Wal, R. S. W., Smeets, C. J. P. P., Boot, W., Stoffelen, M., Van Kampen, R., Doyle, S. H., Wilhelms, F., Van Den Broeke, M. R., Reijmer, C. H., Oerlemans, J., and Hubbard, A.: Self-regulation of ice flow varies across the ablation area in south-west Greenland, Cryosphere, 9, 603–611, https://doi.org/10.5194/tc-9-603-2015, 2015.

Weinstein, M. and Rao, A. V.: ADiGator: A MATLAB Automatic Differentiation Tool, https://sourceforge.net/projects/adigator/, 2011-2016.

Werder, M. a., Hewitt, I. J., Schoof, C. G., and Flowers, G. E.: Modeling channelized and distributed subglacial drainage in two dimensions, Journal of Geophysical Research: Earth Surface, 118, 2140–2158, https://doi.org/10.1002/jgrf.20146, http://doi.wiley.com/10.1002/jgrf.20146, 2013.

Zwally, H. J., Abdalati, W., Herring, T., Larson, K., Saba, J., and Steffen, K.: Surface melt-induced acceleration of Greenland ice-sheet flow., Science (New York, N.Y.), 297, 218–22, https://doi.org/10.1126/science.1072708, http://www.sciencemag.org/cgi/doi/10.1126/science.1072708http://www.ncbi.nlm.nih.gov/pubmed/12052902, 2002.